Technical Report Documentation Page

1. Report No. ABC-UTC-2016-C3-UNR03-Final	2. Government Accession No.	3. Recipient's Catalog No.	
4. Title and Subtitle **Application of Methacrylate Polymers for Seismic ABC Connections**		5. Report Date June 2022 6. Performing Organization Code UNR	
7. Author(s) Mahmoud Aboukifa, Mohamed Abokifa, Mohamed A. Moustafa (https://orcid.org/0000-0002-1006-7685)		8. Performing Organization Report No.	
9. Performing Organization Name and Address Department of Civil and Environmental Engineering University of Nevada, Reno 1664 North Virginia Street Reno, Nevada 89557-0152		10. Work Unit No. (TRAIS) 11. Contract or Grant No. 69A3551747121	
12. Sponsoring Organization Name and Address Accelerated Bridge Construction University Transportation Center Florida International University 10555 W. Flagler Street, EC 3680 Miami, FL 33174 US Department of Transportation Office of the Assistant Secretary for Research and Technology And Federal Highway Administration 1200 New Jersey Avenue, SE Washington, DC 201590		13. Type of Report and Period Covered Final Report 06/01/2020-12/31/2021 14. Sponsoring Agency Code	
15. Supplementary Notes Visit www.abc-utc.fiu.edu for other ABC reports.			
16. Abstract Accelerated bridge construction (ABC) has several advantages, such as reducing onsite construction time, reducing the traffic congestion around construction sites, and improving the quality of the prefabricated elements for both new bridges or rehabilitation or replacement of old bridges. ABC is considered a good and efficient candidate to replace the cast-in-place (CIP) conventional on-site construction techniques. ABC has been widely used in low seismic regions mostly in the superstructure elements. However, ABC is not widely implemented in the substructure elements such as column-base connections, especially in moderate and high seismic regions due to the uncertainty in the seismic performance of the substructure connections. Few ABC seismic connections were developed and have been demonstrated for potential use in high seismic regions. Among these is ultra-high performance concrete (UHPC) filled-duct connection. The use of the very expensive proprietary UHPC poses a great challenge for wider implementation of this type of connection. The overall goal of this study was to find an efficient and feasible alternative for the grouting material (i.e., polymer concrete) used in such connection as well as examining its usage in the seismic connection of precast bridge columns that can emulate the seismic performance of conventional CIP connections. Reducing mixing complexity, costs and time required by the grouting material to gain full-strength was the focus of this study to establish an efficient and less restrictive alternative for UHPC-filled grouted-duct connections. In the first phase of this project, a comprehensive study of the mechanical properties of the polymer concrete material was conducted to provide the basic understanding of its structural behavior on the material level. Given its observed satisfactory performance, the polymer concrete mix was further used and incorporated into grouted-filled duct connection of a 42%-scale column model to connect the precast columns to footings. The column model was tested to failure under combined axial and cyclic lateral loading to investigate its seismic performance and evaluate its ability to emulate the seismic performance of the CIP system. Overall, the polymer concrete-filled duct connection, as described in this study, has successfully demonstrated an acceptable seismic performance and are, in turn, recommended as suitable precast column-to-footing or column-to-cap beam connections for moderate and high seismic regions. Using such connection with the polymer concrete mix can assure the formation of full plastic moment in columns without any connection damage.			
17. Key Words Polymer Concrete, Grouted Ducts, Large-scale Column Test, Seismic Response		18. Distribution Statement No restrictions.	
19. Security Classification (of this report) Unclassified.	20. Security Classification (of this page) Unclassified.	21. No. of Pages 65	22. Price

(this page is intentionally left blank)

APPLICATION OF METHACRYLATE POLYMERS FOR SEISMIC ABC CONNECTIONS

Principal Investigators: Mohamed A. Moustafa

Department of Civil and Environmental Engineering

University of Nevada, Reno

Authors

Mahmoud Aboukifa

Mohamed Abokifa

Mohamed A. Moustafa

Sponsored by

Accelerated Bridge Construction University Transportation Center

A report from

University of Nevada, Reno Department of Civil and Environmental Engineering, MS 258 1664 N. Virginia St.

Reno, NV 89557

www.unr.edu/cee

June 2022

DISCLAIMER

The contents of this report reflect the views of the authors, who are responsible for the facts and the accuracy of the information presented herein. This document is disseminated in the interest of information exchange. The report is funded, partially or entirely, by a grant from the U.S. Department of Transportation's University Transportation Program. However, the U.S. Government assumes no liability for the contents or use thereof.

ABSTRACT

Accelerated bridge construction (ABC) has several advantages, such as reducing onsite construction time, reducing the traffic congestion around construction sites, and improving the quality of the prefabricated elements for both new bridges or rehabilitation or replacement of old bridges. ABC is considered a good and efficient candidate to replace the cast-in-place (CIP) conventional on-site construction techniques. ABC has been widely used in low seismic regions mostly in the superstructure elements. However, ABC is not widely implemented in the substructure elements such as column-base connections, especially in moderate and high seismic regions due to the uncertainty in the seismic performance of the substructure connections. Few ABC seismic connections were developed and have been demonstrated for potential use in high seismic regions. Among these is ultra-high performance concrete (UHPC) filled-duct connection. The use of the very expensive proprietary UHPC poses a great challenge for wider implementation of this type of connection. The overall goal of this study was to find an efficient and feasible alternative for the grouting material (i.e., polymer concrete) used in such connection as well as examining its usage in the seismic connection of precast bridge columns that can emulate the seismic performance of conventional CIP connections.

Reducing mixing complexity, costs and time required by the grouting material to gain full-strength was the focus of this study to establish an efficient and less restrictive alternative for UHPC-filled grouted-duct connections. In the first phase of this project, a comprehensive study of the mechanical properties of the polymer concrete material was conducted to provide the basic understanding of its structural behavior on the material level. Given its observed satisfactory performance, the polymer concrete mix was further used and incorporated into grouted-filled duct connection of a 42%-scale column model to connect the precast columns to footings. The column model was tested to failure under combined axial and cyclic lateral loading to investigate its seismic performance and evaluate its ability to emulate the seismic performance of the CIP system. Overall, the polymer concrete-filled duct connection, as described in this study, has successfully demonstrated an acceptable seismic performance and are, in turn, recommended as suitable precast column-to-footing or column-to-cap beam connections for moderate and high seismic regions. Using such connection with the polymer concrete mix can assure the formation of full plastic moment in columns without any connection damage.

ACKNOWLEDGEMENTS

This project was supported by the Accelerated Bridge Construction University Transportation center (ABC-UTC at www.abc-utc.fiu.edu) at Florida International University (FIU), as lead institution, and Iowa State University (ISU), University of Nevada, Reno (UNR), University of Oklahoma (OU), and University of Washington (UW) as partner institutions. The authors would like to acknowledge the ABC-UTC support.

The authors would like to extend special appreciation to the ABC-UTC and the U.S. Department of Transportation Office of the Assistant Secretary for Research and Technology for funding this project. The authors would like to thank the Research Advisory Panel members Mr. Mike Stenko from Transpo Inc. and Ron Bromenschenkel from Caltrans. The donation of the polymer concrete by Transpo® which is greatly acknowledged. The experimental studies would not have been possible without the support of UNR Earthquake Engineering Laboratory staff members Dr. Patrick Laplace, Mark Lattin, Chad Lyttle and Todd Lyttle. The research team would like to thank everybody involved in the project.

TABLE OF CONTENTS

LIST OF TABLES

LIST OF FIGURES

CHAPTER 1. INTRODUCTION

1.1. Overview

Accelerated bridge construction (ABC) techniques has become a great interest and the preferred choice in many departments of transportation (DOTs) throughout the United States over the past few decades. However, most of the currently used ABC techniques are in the non-seismic-critical members such as superstructure members. ABC as a technology includes several techniques such as using self-propelled modular transporters (SPMTs) and slide-in for moving bridges into its final position for instance. Other ABC technologies include offsite prefabrication of structural components, shipping to the construction site and finally assembling of these prefabricated elements on site. Numerous advantages could be achieved by implementing the ABC techniques in the construction of new bridges or the rehabilitation and replacement of old deteriorated bridges. Reducing onsite construction time, reducing the traffic congestion around the construction sites, and improving the quality of the prefabricated elements are the main advantages of ABC technology. Currently, there are many research efforts which focused on introducing the ABC technology to the seismic-critical members such as substructure elements (i.e., columns and footings).

The main challenge facing the adoption of the ABC technology in moderate and high seismic areas is the uncertainty in the adequacy of precast member connections to maintain the integrity of the structure under cyclic loads. It is important to develop ABC systems that can emulate conventional cast-in-place (CIP) construction systems because, if this can be achieved, typical analysis and design procedures can be used. The main difficulty with developing emulative systems is the detailing of connections because of their critical role in transferring forces and maintaining stability of the structure. Substructure connections, in particular, are critical in high seismic zones as they have to dissipate energy through significant cyclic nonlinear deformations while maintaining their load capacity and their integrity within the structural system.

There are several types of ABC substructure connections that have been developed in recent years such as, grouted-duct connections, pocket-type connections, and column-in-socket connections. The study presented in this report focuses on grouted-ducts connection, which is one of the most promising types. This connection is sometimes called non-coupled plunged connections or referred to as precast column with no couplers (PNC) detail for column-to-footing and column-to-cap

connections. A grouted duct connection comprises a precast column with extended straight longitudinal reinforcing bars that are anchored in grouted corrugated ducts installed in the connecting members (footing or cap beam). A schematic representation of a grouted duct column-to-footing connection detail is shown in Figure 1.1. Past research by Tazarv and Saiidi (2015), and Aboukifa et al. (2021) has demonstrated the seismic performance of the grouted duct connection and demonstrated its validity with advanced construction materials. However, such development used a proprietary and non-proprietary ultra-high performance concrete (UHPC) mixes which were relatively expensive, and very complex to mix. The proprietary nature pose challenges for specification writers while high initial costs and complex mixing procedures present an obstacle for the adoption of ABC by the bridge engineers.

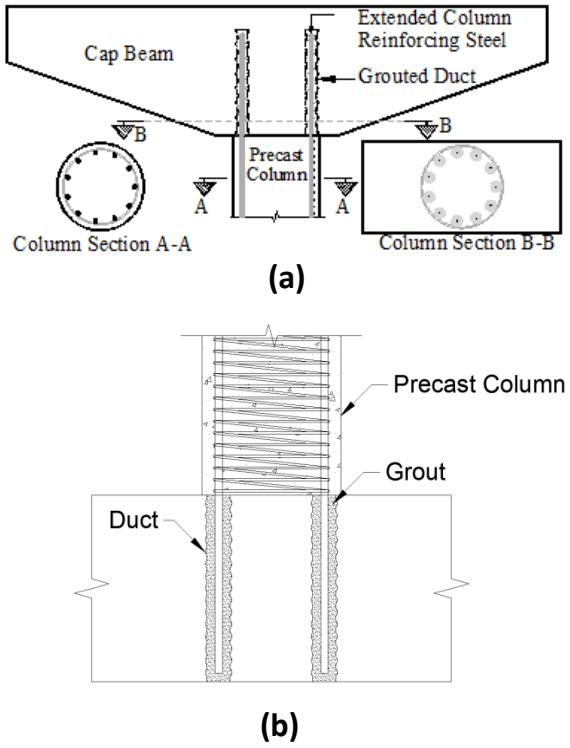

Figure 1.1 Schematic of Grouted Duct Connections: (a) Column to Cap Beam Connection, (b) Column to Footing Connection (adopted from Shrestha et al. 2018).

The goal of this research is to evaluate the seismic performance of grouted-duct connections using polymer concrete mix that could replace UHPC without affecting the structural behavior of such connections. To achieve this goal, research was conducted to provide the basic understanding of the mechanical properties of the polymer concrete mix in the first phase of this project. The large-scale column test and demonstration for seismic performance of the ABC connection was carried

out in the second phase of the project as discussed in this report. It is noted that the polymer concrete mix used in this study is less expensive, and more efficient alternative to UHPC for such connections.

1.2. Previous Studies

Many bridge substructure and superstructure members can be built offsite and then assembled on-site using different types of precast connections. In high seismic zones, these connections are very critical and need to be well designed and constructed to be able to emulate the CIP connections. To produce emulative systems, ABC connections should maintain their load capacities while undergoing large cyclic deformations of adjoining members. This is even more challenging for bridge columns since these elements are required by most of the design specifications to undergo high plastic deformations during large seismic events. This study focuses on earthquake-resistant ABC connections for bridge columns using grouted ducts.

Marsh et al. (2011) investigated the seismic performance of seven types of precast column connections in moderate and high seismic regions: (1) bar couplers, (2) grouted ducts, (3) pocket connections, (4) member socket connections, (5) hybrid connections, (6) integral connections, and (7) emerging technologies. The authors showed that the precast concrete bridge pier systems have developed an emulative seismic behavior to the monolithic systems and they undergo similar damage to the monolithic systems due to the formation of plastic hinges in columns. A comprehensive literature review on the description of these seven types of connections beside their available experimental studies was conducted and presented by Tazarv and Saiidi (2014). For the purpose of the study presented herein, an updated literature search is conducted on the grouted-duct connections to include recent efforts done towards the implementation of this type of connection through the experimental testing of large-scale columns incorporating the grouted-duct connection in their column-footing connections.

Matsumoto et al. (2001) tested a full-scale precast cap beam connected to a representative portion of a column using the grouted-duct system. The column was reinforced longitudinally with 4 epoxy-coated bars of #9 diameter and transversely with #3 spirals spaced at 4 in. resulting in reinforcement ratios of 0.57% for the former and 0.46% for the latter. The small representative part of the column had a clear height of only 24 in while the diameter was 30 in. The embedment length of the bars in the ducts was 15 in and traditional high-strength grout was used for the

connections. The specimen was tested using two vertical and one horizontal loading rams to obtain the load-deflection of the connection at the service and failure levels under different moment demands. The test results showed that the grouted-duct connection exhibited the same load-deflection response as the cast-in-place column model with the same expected strength, ductility, and bar anchorage.

Pang et al. (2008) did a comparative experimental study between 40% scale models of CIP and grouted-duct connection with the same scale and reinforcement ratios. The column diameter and height were 20 in and 60 in, respectively. The columns were tested under 8% axial load ratio and cyclic lateral loading till failure. The test results showed that the behavior of the grouted-duct connection was the same as the CIP connection. Both columns exhibited the same failure mode of bars buckling then bars rupture. The only observed difference between both columns is that the CIP column model had better crack distribution along the column than the precast connection which was observed to have a concentrated one large crack at the column-beam interface. Restrepo et al. (2011) tested a series of 42% scale column-cap beam connection incorporating different ABC techniques suitable for seismic zones. One of these connections was utilizing the grouted-ducts (GD). The column height was 45 in. while the column diameter was 20 in. The specimen was tested under cyclic lateral loading. Test results showed that the GD column model exhibited an emulative behavior to the CIP column model with stable hysteretic behavior. the GD column model showed an acceptable ductile behavior with a displacement ductility of 8 which was approximately 80% of that of the CIP column model.

Belleri and Riva (2012) tested a column model utilizing the grouted-duct connection (with traditional grouts again like most of the previous studies above) but unlike the traditional setting, the ducts were laid out in the column and the rebars were protruding out of the footing. The column height was 126 in and the column diameter was 15.75 in. The embedment length into the footing was 45.25 in. The test results showed that the grouted steel ducts are suitable to be used in seismic regions and can develop high ductile behavior. The authors also claimed that the post-seismic repair of these connection may be simpler than CIP or pocket foundation connections. The authors suggested to use an unbonded length of projecting bars at the column-footing interface to increase ductility and reduce damage. Popa et al. (2015) tested two sets of columns under two different axial load level under cyclic lateral loading till 5% drift ratio. Each set consisted of two precast columns utilizing the grouted-duct connection and one CIP column. The grouted ducts were laid

out inside the precast columns while the bars were protruding out of the footing. The test results showed that a similar hysteretic response was for both, the precast and the CIP, specimens for each level of applied axial force. Furthermore, all the precast columns were observed to show less severe final damage state than that obtained for the CIP specimens

Tazarv and Saiidi (2015) investigated the seismic performance of a precast column utilizing the grouted-duct connection using UHPC instead of high strength grout as a filler. A half scale bridge column was tested under axial load and cyclic lateral loading and then its seismic behavior is compared to a similar CIP column. The authors concluded that the UHPC-filled duct connections are emulative of the conventional CIP column-footing connection as the plastic moment capacity of the column is developed and a high drift capacity is achieved without connection failures such as bar pullout, duct pullout or concrete breakout failure. The test results also showed that the mode of failure, base-shear capacity, and strength and stiffness degradation of this connection were nearly the same as those of CIP.

Aboukifa et al. (2021) investigated the cyclic performance of two precast column models utilizing the grouted-duct connection using in-house developed non-proprietary UHPC as a grouting material. Two half scale bridge column were tested under axial load and cyclic lateral loading and then their seismic behaviors were compared to a similar column with proprietary UHPC-filled ducts. The authors concluded that the non-proprietary UHPC-filled duct connections were successful to emulate conventional CIP column-footing connection and to substitute the very expensive proprietary UHPC without increasing the anchorage length of the column dowels inside the footing.

1.3. Objectives

The overall goal of the present study was to find a more efficient alternative to UHPC (i.e., polymer concrete) and evaluate columns that utilize it in grouted-duct connection. This was done with the understanding that the compressive strength of the polymer concrete could be much lower than that of standard UHPC. Reducing the mixing complexity and time as well as gaining full strength rapidly was the focus of the study to establish a less expensive, less restrictive, and more efficient alternative for ABC column connections. To achieve this goal, research was conducted to provide the basic understanding of the mechanical properties of the polymer concrete mix (phase one) and

examine its validity for usage in a large-scale column under cyclic testing for ultimate validation of the material and connection (phase two).

The objective of phase two of the study was to conduct an almost half-scale column test at UNR Earthquake Engineering Laboratory under axial and cyclic lateral loading to investigate its cyclic performance. The column model implemented the polymer concrete duct connection detail. Thus, the objective of the test was to evaluate the ability of the ABC column to emulate the seismic performance of the CIP system. The column model used the same detail (i.e., same connection type and anchorage length) as that used in previously tested literature columns which incorporated UHPC-filled grouted duct connections.

1.4. Report Outline

This report consists of five chapters. The report starts with an introduction to ABC techniques and the grouted-duct connection. Furthermore, an overview of relevant literature is presented in Chapter 1. The polymer concrete material properties with regards to the mix proportions, compressive, tensile, and flexural behaviors are shown in Chapter 2. The Design procedure, structural detailing, and testing loading protocol for the large-scale column model test is provided in Chapter 3. The comprehensive discussion of the column test results is presented in Chapter 4. The cyclic performance evaluation of the tested column model with respect to similar literature column models, CIP column model, PNC with proprietary UHPC column model, and S1-Bond with non-proprietary UHPC column model is also presented in Chapter 4. Finally, a summary of findings and conclusions is presented in Chapter 5.

CHAPTER 2. MATERIAL PROPERTIES

2.1. Introduction

This section provides results of the main mechanical characterization tests of the materials which were used in this study. As mentioned earlier, the advantage of using PMMA-PC for the grouted column ducts is that it has a high early strength as it can reach the full strength in less than 24 hours. This makes this material ideal solution for various ABC field joint applicatons and fast repair applications. However, up to the date of this writing, this material is still uncommon and there are only limited information about the early strength and behavior of this material. Hence, this section summarizes the main results of the early mechanical characterization tests of the PMMA-PC. The early strength and behavior assessment of this material included compression and flexure tests. Moreover, this section shows the compressive strength results of the conventional concrete which was used for the fabrication of the column and footing. The results of the rebar coupon tension testing of the A706 Grade 60 reinforcement were also reported at the end of this section. Nonetheless, this chapter also provides information about the mixing procedure and mixing proportions of the PMMA-PC.

2.2. Poly-Methyl Methacrylate Polymer Concrete (PMMA-PC)

PMMA-PC has physical and mechanical properties which are very comparable to that of the high strength concrete. The flow properties and color of the PMMA-PC are closely similar to the cementitious based types of concrete. While, PMMA-PC has no cement or cement-based products in its composition. The composition of the PMMA-PC includes mixing of Methyl Methacrylate resin with a Benzoyl Peroxide initiator in addition to an optional graded aggregate of 3/8 x 3/16 nominal maximum size. Adding aggregate to the mix is only recommended for applications in which the thickness of the patch exceeds about 1.25 in and concrete should be used rather than a mortar (e.g., full-depth field joints in bridge decks). However, the PMMA-PC paste can also be used without aggregates in tight and narrow applications such as grouted column ducts and repairing and patching purposes.

The commercial name of the PMMA-PC material which was used in this study is Transpo® T-17 PC and it is one of the products of Transpo Industries Incorporation. The specified compressive strength of the PMMA-PC is about 8.0 ksi after 24 hours and the specified tensile strength is 1.0-1.2 ksi which usually is achieved at 1 to 3 days. The T-17 PC was designed for use on new

construction and rehabilitation of bridge decks, expansion joints, bearing pads, and patching of airport runways. This material is ideal for these applications due to its fast setting, high bond strength, and early strength. The T-17 PC has been used for decades in many projects around the nation. This class of materials are usually more available around the United States and Canada relative to other emerging materials like UHPC. The commercial T-17 PC product is usually packed in pre-packed bags and liquid pails.

2.2.1. Mixing Proportions and Methodology

PMMA-PC is commonly packed into two different components as follows: (1) T-17 powder constituents which are packed in 50-lbs bags and consists of a proprietary blend of sand, inert fillers, polymers, and initiators (see Figure 2.1a); (2) T-17 liquid admixture which is packed in 1 or 5-gallon pails and consists of a solvent-free 100% reactive low viscosity methyl methacrylate (MMA) (see Figure 2.1b).

Figure 2.1 Transpo® T-17 PC Components (a) T-17 powder, and (b) T-17 liquid component.

Table 2.1 shows the mixing proportions of the Transpo® T-17 PC based on the number of powder bags that are used on a single batch. Table 2.2 shows the mix components and quantities per cubic yard and cubic meter of the Transpo® T-17 PC. The T-17 PC was mixed in 5-gallon buckets using a hand drill mixer as shown in Figure 2.2. The T-17 PC can also be mixed in large quantities up to 4.0 ft^3 using the conventional rotary drum mixers

Table 2.1 Transpo® T-17 PC Mixing Proportions According to the Number of T-17 Powder Bags.

No. of T-17 powder bags per batch	1	2	3	4	5	6
T-17 powder (lb)	50	100	150	200	250	300
T-17 liquid (lb)	4.77	9.54	14.31	19.08	23.85	28.62
T-17 liquid (gallon)	0.63	1.25	1.88	2.50	3.13	3.75
Batch volume (ft^3)	0.4	0.8	1.2	1.6	2.0	2.4

Table 2.2 Transpo® T-17 PC Mixing Proportions Per Cubic Yard and Cubic Meter.

	kg/m^3	lb/yd^3	Percentage per weight (%)
T-17 powder	2002	3375	91.3
T-17 liquid	191	322	8.7

The mixing methodology of the T-17 PC is divided into three main steps (see Figure 2.2) as follows: (1) all amount of the T-17 liquid component is added to the bucket; (2) the T-17 powder bags are then added gradually over the course of 1 minute while mixing. (3) Mixing is continued for another 3 minutes until uniform consistency to ensure appropriate PMMA-PC paste. The typical mixing time for the T-17 PC is about 4 minutes for one batch or one bucket. As mentioned earlier, this material was designed for quick repairs and patching as it has a very high early strength. Hence, it is important to note that this material has a relatively short working time after mixing which usually ranges between 20 to 30 minutes. This material has a wide application temperature range which ranges between 14 to less than 100 °F. This material is also flowable, hence it is ideal for use in narrow applications or structural applications with dense reinforcement. This material does not require any special vibration processes which are usually used to expel the entrapped air inside the fresh conventional concrete. In general, the T-17 PC does not require any special considerations for surface finishing, and it follows the same finishing procedure as the typical conventional concrete. Steel trowels, floats, or screeds can be used to obtain a closed and flat surface while tinning or broom finishing is not recommended.

Figure 2.2 Mixing of T-17 PC.

2.2.2. Early Strength Characterization of PMMA-PC

2.2.2.1. Compression strength and behavior

As previously mentioned, PMMA-PC has been used in previous studies conducted by the authors. In these studies, small aggregates have been added to the PMMA-PC mixes and used inside the precast bridge deck field joints. Moreover, these previous studies have investigated and reported the main mechanical properties of these PMMA-PC mixes with aggregates. While the PMMA-PC mixes which are used in the current study have no aggregates in their composition. Hence, it was important to understand the main mechanical properties, especially early strength assessment of

these mixes through mixing and testing a trial batch. A trial batch of PMMA-PC without aggregates has been mixed before the fabrication of the specimen. The main purpose of this trial batch is to understand the early strength and behavior of the developed mixes and determine the proper time for conducting the large-scale testing of the column-footing specimen. The preliminary test plan was set up based on conducting the large-scale testing within one week from pouring the PMMA-PC inside the column ducts.

Hence, twelve 3x6 in cylinders were prepared from the trial batches to be tested at different ages (i.e., 1, 2, 3, and 7 days). The compression testing of cylinders at 7 days was delayed to 9 days because of a malfunction of the testing machine. Three specimens were prepared for testing at each age to test the consistency of the results of this material. More test cylinders were also prepared from the batches which were used inside the grouted ducts of the large-scale specimen. The test cylinders were left to cure at the fabrication yard to be exposed to the normal site conditions. The top surface of the test cylinders was flattened using flat trowels. Hence, no special preparation such as end capping, end cutting, or grinding were required for any of the test cylinders.

A SATEC compression machine with a maximum compression capacity of 500 kips and a Tinius Olsen machine was used to test the PMMA-PC cylinders according to the ASTM standards C469. The test cylinders were loaded up to failure at a rate of 250 lb/sec. Three displacement transducers (i.e., LVDTs) were used during the test to measure the relative displacements between the two-cylinder ends. The average of the readings from the three LVDTs were used to predict the compressive strains of the test cylinders. The main aim for using this test setup is to get the full stress-strain curve of this new material and determine the static modulus of elasticity. The compression testing of the PMMA-PC cylinders and a sample of the compression damage of cylinders at 3 Days are shown in Figure 2.3. A summary of the measured compressive strength of the PMMA-PC at different ages is reported in Table 2.3. The reported compressive strength is the average of a minimum of three-cylinder samples tested at each testing date. All cylinders from both trial batch and actual material using for the column assembly were cured under ambient conditions at construction site at UNR. Thus, it is noticed that the average compression strength at different ages was slightly higher for trial batch cylinders than the batch used for column because of the slightly varying ambient temperatures during curing.

Figure 2.3 Compression Testing and Sample of Damage of the PMMA-PC 3x6 in Cylinders.

Table 2.3 Measured Compressive Strength of the PMMA-PC.

Batch	Test Date	Machine load (lb)	Average load (lb)	Average stress (ksi)
Trial PMMA-PC Batch	1 Day	51,725	53,147	7.52
		52,415		
		55,300		
	2 Days	54,620	52,040	7.36
		51,065		
		50,435		
	3 Days	44,290	49,033	6.95
		48,360		
		54,450		
	9 Days	52,370	51,966	7.39
		56,877		
		46,652		
PMMA-PC for grouted column ducts	3 Days	48,125	49,058	7.04
		47,795		
		51,255		
	14 Days (Test Day)	51,745	50,362	7.20
		50,365		
		48,975		

Figure 2.4 shows the obtained compressive stress-strain relationships of the trial PMMA-PC batch at different ages. While Figure 2.5 shows the compressive stress-strain relationships of the PMMA-PC which was used for the grouted column ducts. The modulus of elasticity of the PMMA-PC was calculated based on the stress and strain values that correspond to 10% and 30% of the ultimate

compressive strength. The average values of the modulus of elasticity and compressive strength which were obtained from three test samples at each age, were reported in Figures 2.4 and 2.5.

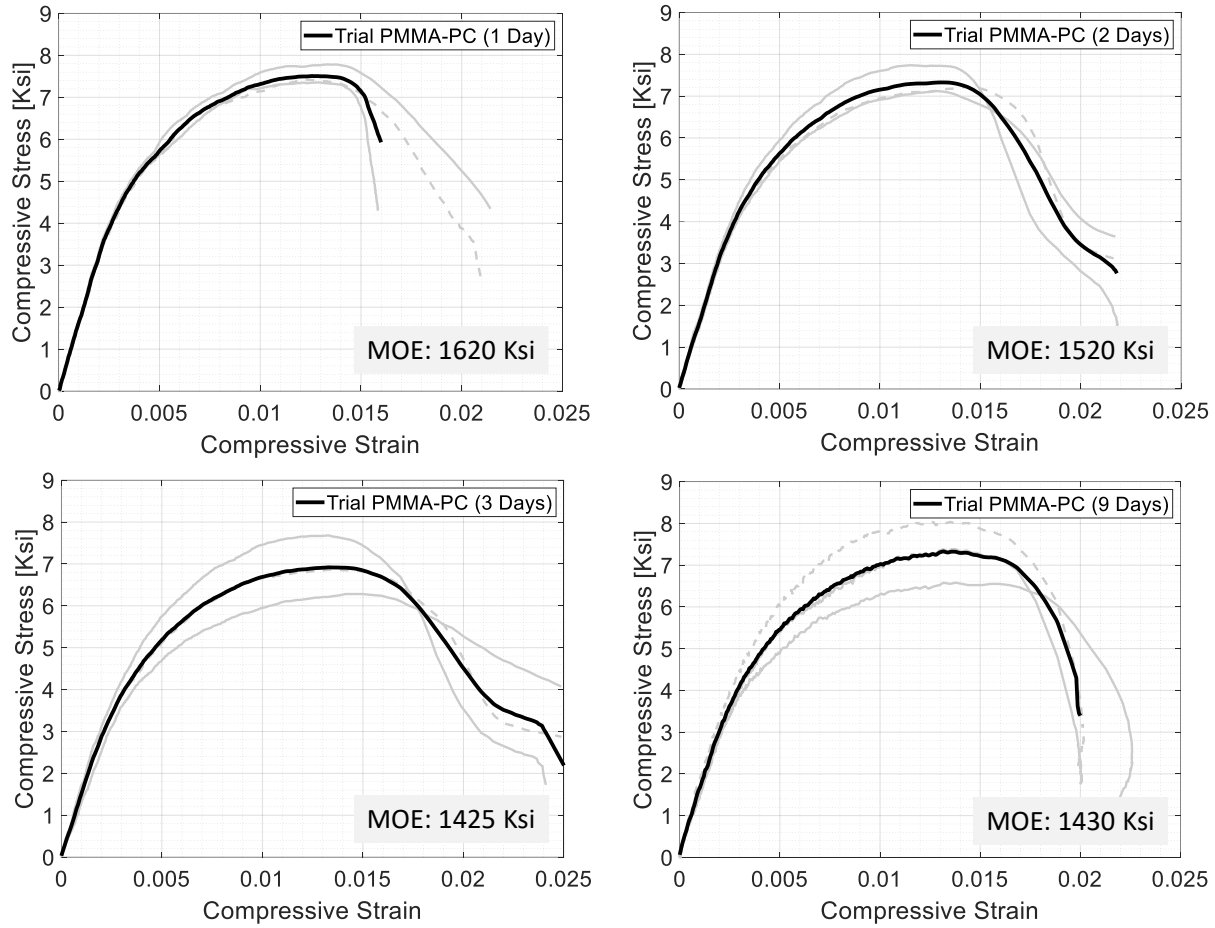

Figure 2.4 Compressive Stress-Strain Relationships of the Trial PMMA-PC Batch.

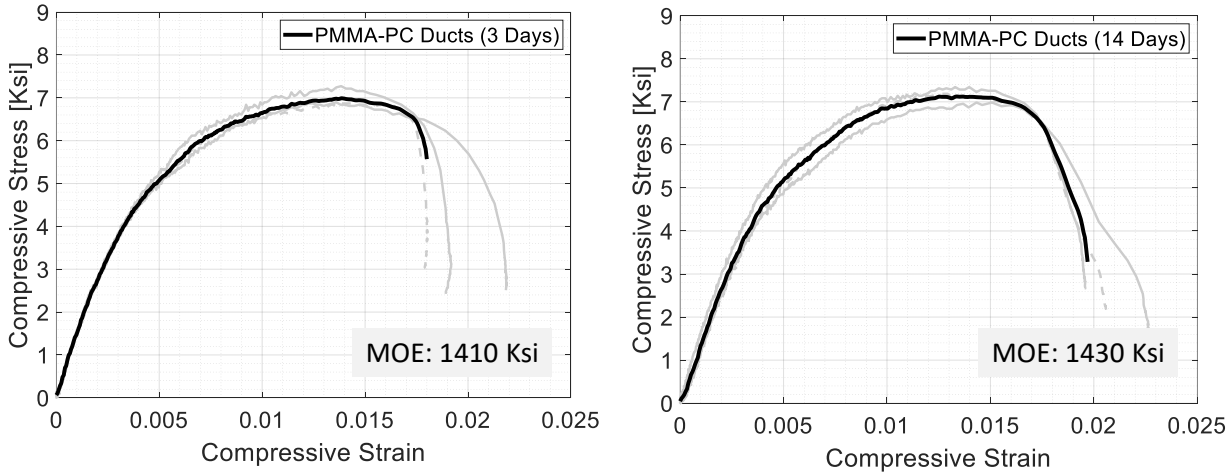

Figure 2.5 Compressive Stress-Strain Relationships of the PMMA-PC Which was used for the Grouted Column Ducts.

The average PMMA-PC compressive elastic modulus was determined to be approximately 1,475 ksi. It can be seen from the previous figures that the PMMA-PC has ultimate strain capacity that can be as high as 0.014, which is larger than typical ultimate strain capacity of conventional concrete. The PMMA-PC can also sustain large strains and axial deformation after reaching the peak load, i.e. favorable post-peak behavior compared to other concretes.

2.2.2.2. Flexural strength and behavior

For the flexural strength and modulus of rupture characterization, 3 x 3 x 12 in rectangular prisms were prepared from the trial PMMA-PC batch. Instron testing machine with maximum capacity of 50 kips was used to test the PMMA-PC prisms according to the ASTM standards C580 – method C as shown in Figure 2.6. The specimens were tested in flexure in a 4-point bending assembly with two vertical loads applied at the third span points of the specimen. The span between the two support points was 9 in. The load was applied at the middle at a displacement rate of 0.0451 in/min. The displacement rate was controlled by the speed of the machine cross head and was based on achieving a strain rate of 0.01 per minute at the top and bottom of the beam. The test specimens were loaded for one cycle till failure. The flexural stress versus deflection relationships of the PMMA-PC specimens at 1 and 7 days are shown in Figure 2.7. The mid-span deflection of the beams was measured using a laser extensometer device. The laser extensometer reads the extension between two fixed laser targets as one target was attached at the middle of the beam and the other was attached at a fixed point over the bending table as shown in Figure 2.6.

The main purpose of the test was to get the flexural strength and determine the modulus of rupture of the PMMA-PC beams. The average flexural strength of the PMMA-PC test specimens after 1 day and 7 days were determined to be 2.31 ksi and 2.57 ksi, respectively. It can be implied from these tests that the flexural strength of PMMAPC beams is higher than the conventional concrete. The failure of the PMMA-PC bending specimens was a brittle failure after the observance of the first crack, which is similar to conventional concrete.

Figure 2.6 Flexural Tests of the Trial PMMA-PC Batch at 1 day and 7 days.

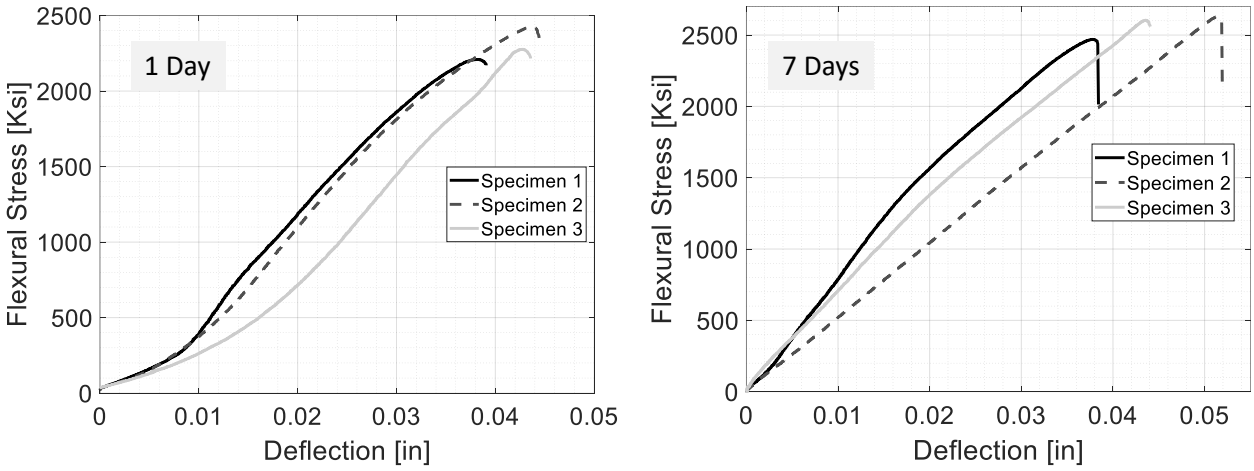

Figure 2.7 Flexural Stress Versus Deflection Relationships of the Trial PMMA-PC Batch at 1 day and 7 days.

2.3. Conventional Concrete

The precast column and footing were fabricated using conventional concrete with 5 ksi specified compressive strength. Both elements were cast using a single batch. Quality control compression test cylinders were prepared from the conventional concrete and left on-site to cure till the specified testing date. The test cylinders were poured into three layers and a tamping steel rod was used to blow each layer 25 times to remove any entrapped air and finally the top surface is flattened using

a spatula. The cylinders were of dimensions 6x12 in. Figure 2.8 shows the pouring of the conventional concrete and the preparation of the test cylinders. The compression testing of the concrete cylinders was done according to the ASTM C39. The test cylinders were loaded to failure at a rate of approximately 35 psi/sec. The compression testing of the conventional concrete cylinders and a sample of compression damage are shown in Figure 2.9.

A summary of the measured compressive strength of the conventional concrete cylinders at different ages is reported in Table 2.4. The reported compressive strength is the average of a minimum of three-cylinder samples tested at each testing date.

Figure 2.8 Preparation of the Conventional Concrete Compression Test Cylinders.

Figure 2.9 Compression Testing of the Conventional Concrete 6x12 in Cylinders.

Table 2.4 Measured Compressive Strength of the Conventional Concrete.

Test Date	Machine load (lb)	Average load (lb)	Average stress (ksi)
7 Days	139,015	137,632	4.87
	137,100		
	136,780		
45 Days (Test Day)	188,930	188,538	6.67
	189,865		
	186,820		

2.4. Reinforcing Steel

Two types of reinforcing steel bars conforming to ASTM A615 and ASTM A706 were used in this study for the transverse and longitudinal reinforcing bars, respectively. Both types are of grade 60. Direct tension tests were performed on four steel coupons from the #3 bars from the same reinforcement batch that was used in our study to determine the actual tensile properties of the reinforcing bars. The samples were tested using the Instron testing machine that has an ultimate tensile capacity of 50 kips. The tensile strains were recorded throughout the test using a laser extensometer and two laser targets attached to each specimen to represent the gage length. One test specimens has only failed inside the gage length (i.e. specimen 3) while the other three specimens were failed outside the gage length. Hence, the full tensile stress-strain relationship up to the ultimate tensile strain was determined based on the results of one specimen only. The yield and ultimate tensile strength in addition to the yield strength of all the specimens are reported in Table 2.5. The measured average yield and ultimate tensile strengths are 80.1 ksi and 113.5 ksi, respectively. The measured average yield and ultimate tensile strains are 0.483 % and 19.68 %, respectively. The tensile stress-strain curve of the #3 reinforcing bars is shown in Figure 2.10 for reference. Moreover, Figure 2.11 shows a typical measured stress-strain curve for a #8 coupon from the columns longitudinal steel, and the summary of the average results from all #8 coupons are tabulated in Table 2.6.

Table 2.5 Results of the #3 Rebar Coupons Tension Tests.

Sample	Ultimate tensile strength (ksi)	Tensile yield strength (ksi)	Tensile yield strain (%)	Tensile rupture strain (%)
1	115.2	83.4	0.487	---
2	112.4	79.2	0.473	---
3	111.1	81.8	0.482	19.68
4	115.2	83.8	0.488	---
Average	113.5	80.1	0.483	19.68

Table 2.6 Measured Tensile Properties of #8 Reinforcing Bars

#8 Bars	f_y (ksi)	$\varepsilon_y\ (in/in)$	$\varepsilon_{sh}\ (in/in)$	f_u (ksi)	$\varepsilon_u\ (in/in)$
	64.05	0.0025	0.0055	106.41	0.141

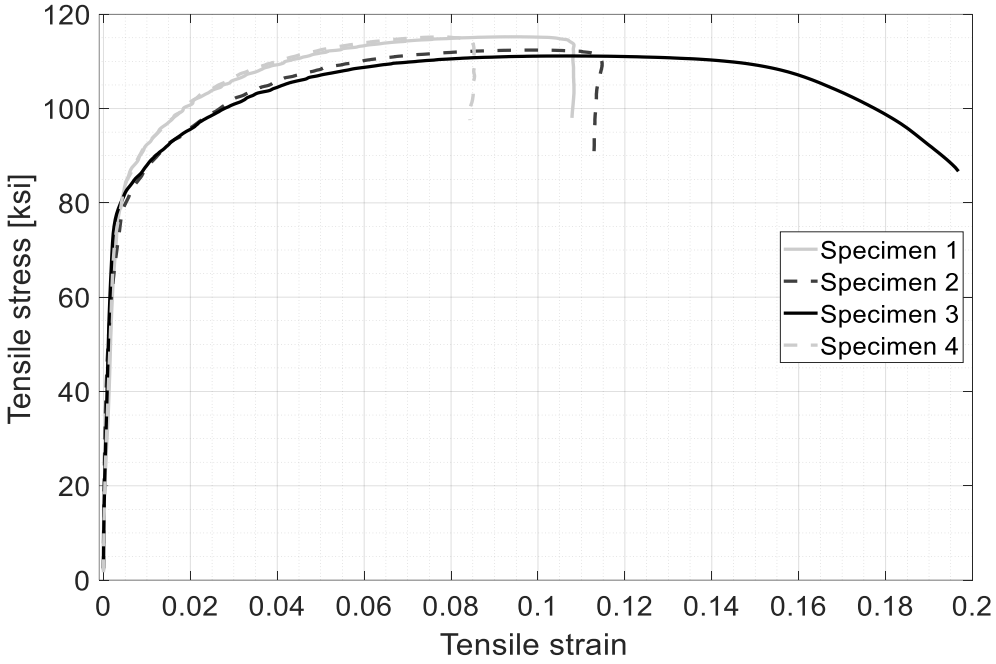

Figure 2.10 Tensile Stress-Strain Curves of the #3 Reinforcing Bars.

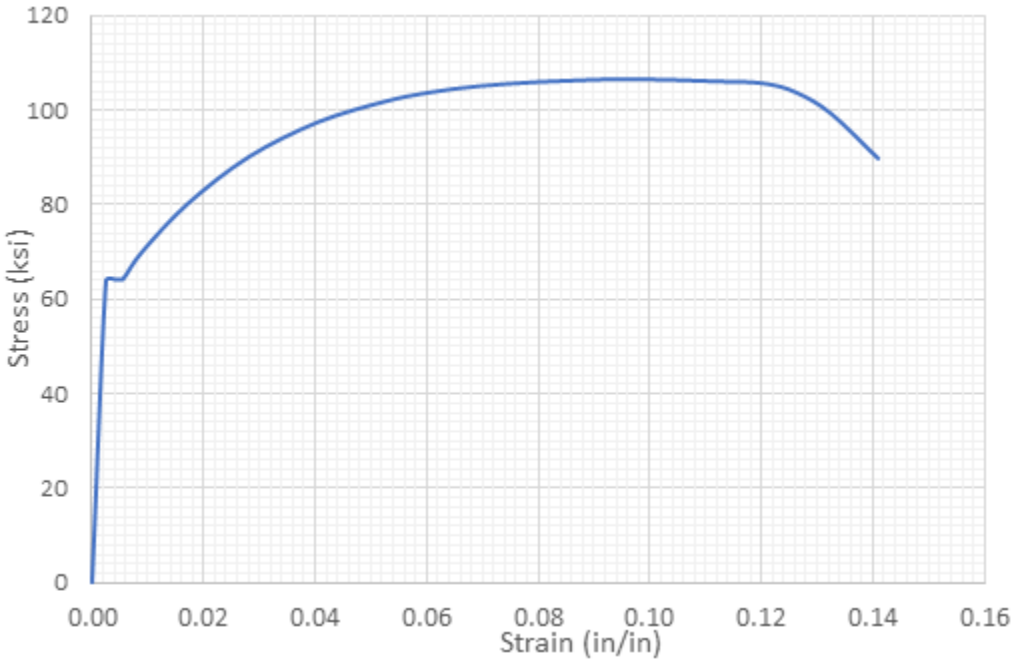

Figure 2.11 Stress-Strain Tensile Relationship of #8 Bars.

CHAPTER 3. EXPERIMENTAL PROGRAM DEVELOPMENT

3.1. Introduction

The seismic design philosophy for the current code allows the bridge columns to undergo inelastic deformations under earthquake loads while maintaining the integrity of the full bridge. In other words, the columns are the bridge's governing structural element in terms of controlling the structural performance during extreme events, such as earthquakes, and the safety and serviceability after the event. When implementing the ABC techniques to accelerate the construction, the columns connections to the footing and the pier cap became very challenging since connections should be able to transfer forces while undergoing large inelastic cyclic deformations.

A large-scale (42%-scale) bridge column with PC filled duct connection to the footing, as shown in Figure 3.1, was designed and tested under axial and cyclic lateral loading at the University of Nevada, Reno (UNR). The objective of the tests was to investigate the seismic performance of duct filled ABC column-to-footing connections using polymer concrete and to assess their potential to replace other very expensive grouting materials like UHPC which is typically used in such connections. The column model is labeled as "PDC" which refers to Polymer concrete-filled Duct Column.

Three more column models from the literature which were also tested at UNR were considered to serve as benchmark models as adopted from Haber et al. (2014), Tazarv and Saiidi (2015), and Aboukifa et al. (2021). The first two models were half scale column models, therefore, they were slightly larger than the models in the study and the column model of Aboukifa et al. (2021). All test models, previous and current, have the same longitudinal and transverse reinforcement ratios. The first column model presented by Haber et al. (2014) was a standard CIP column. The second column presented by Tazarv and Saiidi (2015) and labeled as "PNC" was a precast column with a proprietary UHPC filled duct connection to the footing. The third column model presented by Aboukifa et al. (2021) and labeled as "S1-Bond" was a precast column with a non-proprietary UHPC filled duct connection to the footing. The design of the column models of the present experimental study and the previous three benchmark columns are shown in Table 3.1. The design, construction, Instrumentation, test setup, loading protocol and the material properties

of the PDC column model is presented in this chapter. A short review of the benchmark CIP, PNC, and S1-Bond column models is also presented.

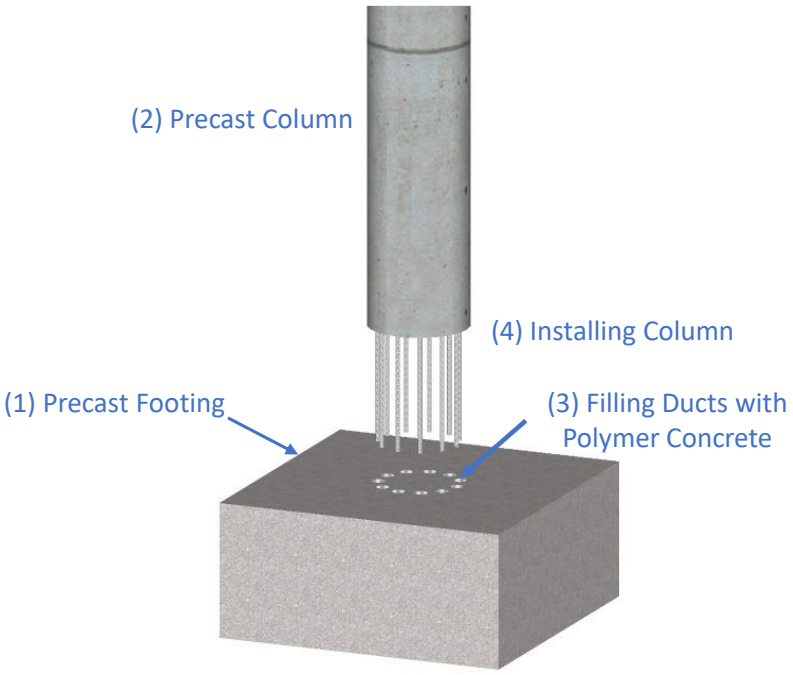

Figure 3.1 PDC Column w/ PC-Filled Duct Connection at Base (Adopted from Tazarv and Saiidi 2014).

Table 3.1 Summary of Column Models Design.

Test		Previous Research at UNR			Present study
Column model		CIP	PNC	S1-bond	PDC
Study		Haber et al. (2014)	Tazarv and Saiidi (2015)	Aboukifa et al. (2021)	This study
Column-footing connection		Monolithic connection	Proprietary UHPC filled ducts	Non-Proprietary UHPC filled ducts	PC filled ducts
Column Dimensions	Diameter [in]	24	24	20	20
	Height [in]	108	108	87	87
	Aspect ratio	4.5	4.5	4.35	4.35
	Clear Cover [in]	1.75	1.5	1	1
	Anchorage [in]	N/A	28	28	28
Reinforcement (Grade 60)	Longitudinal	11-#8	11-#8	8-#8	8-#8
	Ratio ρ_l (%)	1.92	1.92	2.01	2.01
	Transverse	#3 @2in.	#3 @2in.	#3 @2.5in.	#3 @2.5in.
	Ratio ρ_v (%)	1.03	1.03	0.998	0.998
Design Axial Load	Load (kips)	226	200	157	157
	Ratio	10	10	10	10

3.2. Specimens Design and Construction

The cross section of the CIP and PNC column models was circular with a diameter of 24 in and their height was 108 in, while the cross section of the S1-Bond and PDC column models was 20 in, and their height was 87 in. It is noted that the height of the column is measured from the column-footing interface to the axis of the hydraulic actuator used to apply lateral loads. More details about each column are presented next.

3.2.1. CIP Column Model

The CIP column presented by Haber et al. (2014) was a half-scale conventional cast-in-place column model and was designed based on Caltrans Seismic Design Criteria (SDC) version 1.4 (2006) with an aspect ratio of 4.5. The CIP column was constructed to represent a standard bridge column but with a thicker clear cover of 1.75 in. to account for the size of couplers to be used in other columns of the same study, as this column served as the reference column against which the precast columns were compared. The column was reinforced longitudinally with 11-#8 bars and transversely with #3 spirals at a 2 in spacing resulting in longitudinal and transverse steel ratios of 1.92% and 1.03%, respectively. The axial load index, which is the ratio of axial load to the product of column gross section area and the compressive strength of column concrete, was 10%. The specified compressive strength of concrete and yield strength of reinforcements were 5 ksi and 68 ksi, respectively. The column was initially designed for a minimum displacement ductility capacity of 5 but with the final detailing shown in Figure 3.2, the calculated displacement ductility capacity of the column was 7.

3.2.2. PNC Column Model

A half-scale precast column model labeled “PNC” was constructed incorporating the UHPC-filled duct connection. The precast model had a similar geometry, bar size, and bar arrangement to CIP thus its performance was assumed to be emulative of the conventional construction. There was no additional design limitation for PNC with respect to CIP. The PNC column model is shown in Figure 3.3 and the base connection in detail is shown in Figure 3.4. The clear cover in the column was 1.5 in. Corrugated galvanized steel ducts with a nominal 3-inch diameter were used in the footing to be filled with UHPC. The confinement of the duct cage was similar to the column and was provided by #3 spiral spaced at a 2-inch pitch. The column longitudinal bars were extended 28 in at the base for insertion into the ducts. However, the required embedment length was only

19 in based on the design equations recommended for the proprietary UHPC bond length, assuming the concrete compressive strength is 5 ksi, the UHPC compressive strength is 20 ksi, and #8 bars had an ultimate strength of 110 ksi. The duct length was 1 in longer than the extended bar as a construction tolerance. To help spread bar yielding, 4 in of the column longitudinal bars were debonded above and below the column-footing interface as shown in Figure 3.4. Therefore, the effective bar embedment length in the UHPC-filled duct connection of PNC was 24 in, only 5 in. longer than the required development length. To minimize the precast column weight for transportation, hollow core circular section with a 6-inch wall thickness was used at initial stage of construction. After installing the column, the column core was filled with self-consolidating concrete (SCC).

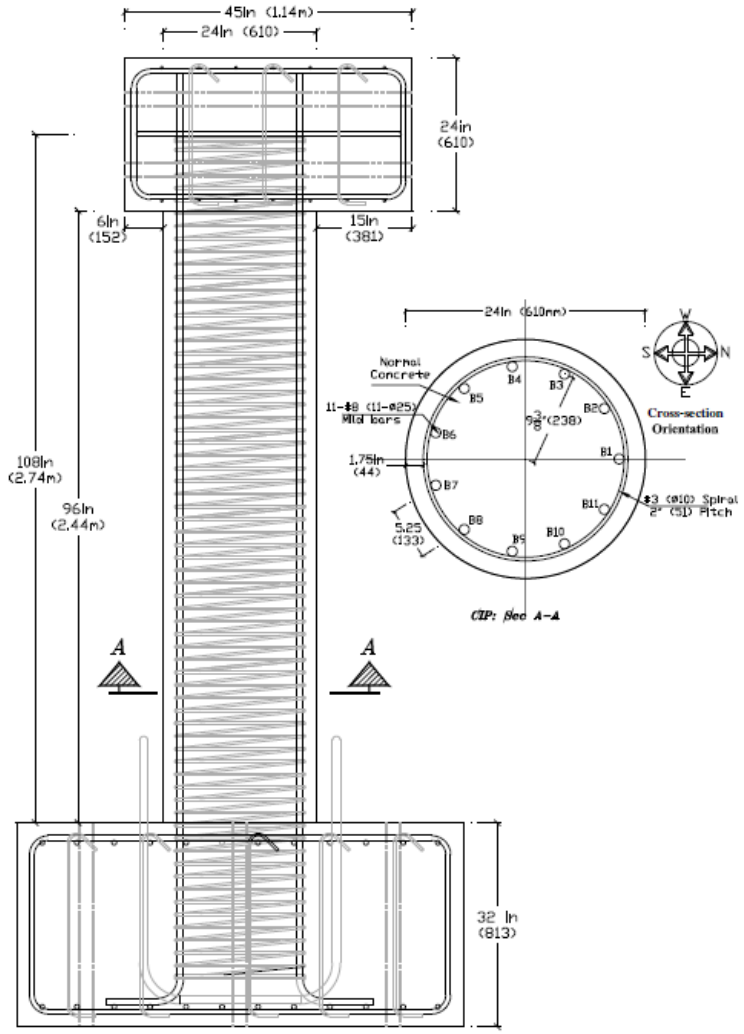

Figure 3.2 CIP Column Model by Haber et al. (2014) [Units: in (mm)] as presented in the study by Tazarv and Saiidi (2014).

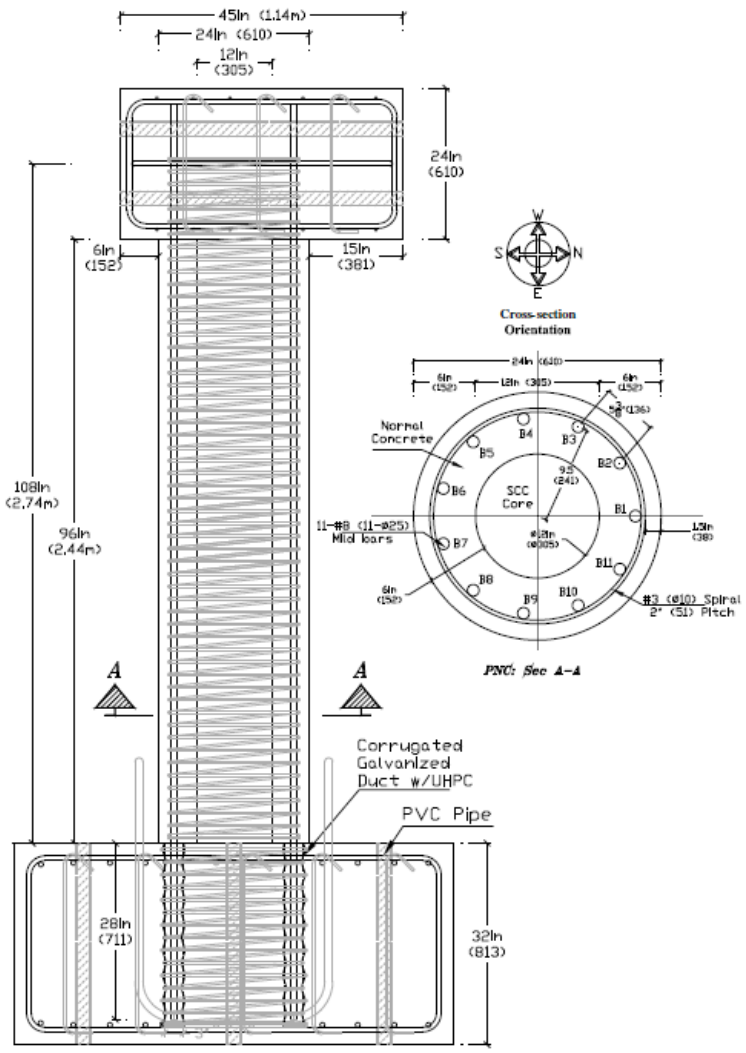

Figure 3.3 PNC Column Model [Units: in (mm)] as adopted from Tazarv and Saiidi (2014).

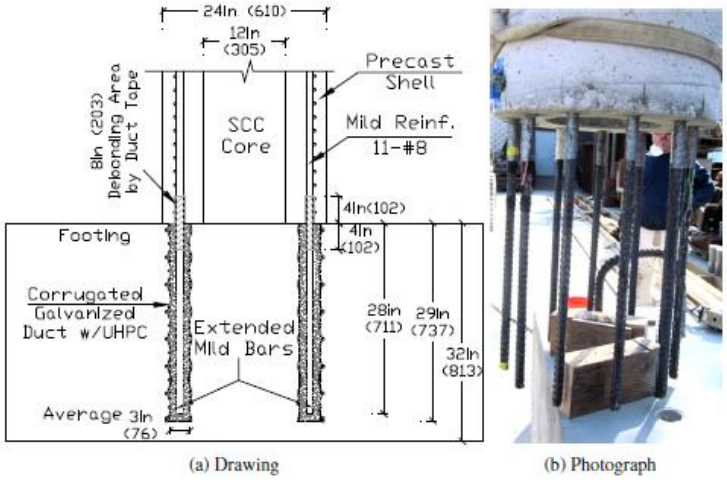

Figure 3.4 PNC Column Base Connection Detail (Adopted from Tazarv and Saiidi 2014).

3.2.3. S1-Bond Column Model

An almost half-scale precast column model (42%-scale) labeled "S1-Bond" was constructed incorporating the non-proprietary UHPC-filled duct connection. The column dimensions shown in Figure 3.5 which are used for both test models, were chosen to have an aspect ratio almost equal to the CIP and PNC column models. The columns height was 87 in, measured from the column footing interface to the to the axis of the hydraulic actuator used to apply lateral loads, while the columns diameter was 20 in and the columns clear cover was 1 in. The precast columns were reinforced longitudinally with 8-#8 bars and transversely with #3 spiral at a 2.5-inch pitch resulting in longitudinal and transverse steel ratios of 2.01% and 0.99%, respectively, to represent similar ratios to the reference column models (CIP and PNC). Corrugated galvanized steel ducts with a nominal 3-inch diameter were used in the footing to be filled with the non-proprietary UHPC. The confinement of the duct cage was similar to the column and was provided by #3 spiral spaced at a 2.5-inch pitch. The embedment length of the column longitudinal reinforcement into the footing was the same as the PNC column model and was equal to 28 in.

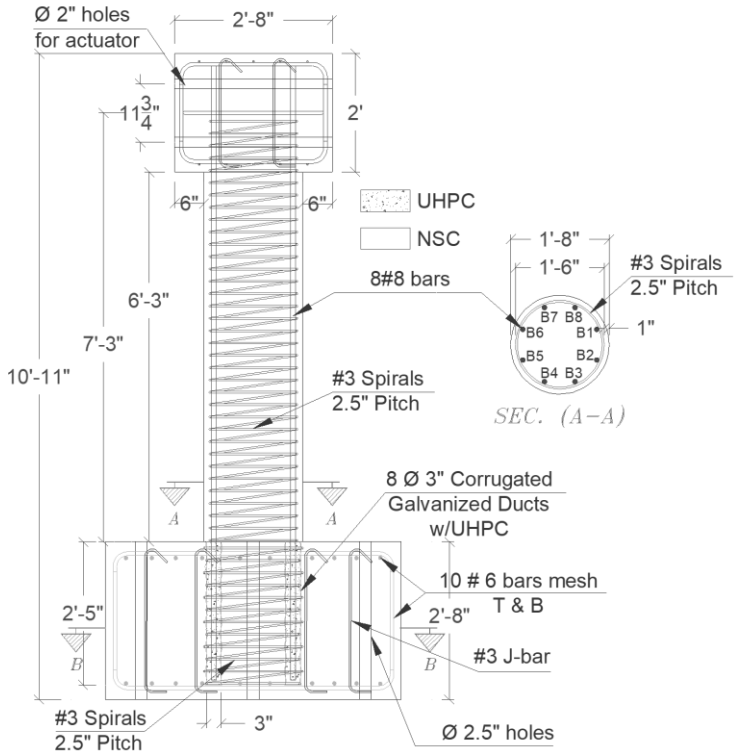

Figure 3.5 S1-Bond Column Model (Adopted from Aboukifa et al. 2021).

3.2.4. PDC Column Model (Current Study)

An exact replicate of the S1-Bond column model was made but with using the Polymer concrete instead of the non-proprietary UHPC as a grouting material for the duct connection. Again, the precast column was of 87 in height and 20 in diameter, while the column clear cover was 1 in. This represents a 42%-scale (almost half scale) of a typical California bridge column. The column dimensions as well as the reinforcement details are shown in Figure 3.6. The precast column was reinforced longitudinally with 8-#8 bars and transversely with #3 spirals at a 2.5-inch spacing, resulting in longitudinal and transverse reinforcement ratios of 2.01% and 0.99%, respectively. These steel ratios are almost corresponding to those of the reference column models of the larger scale (CIP and PNC). The plan dimensions of the footing were 5×5 ft^2 and the depth was 32 in. Corrugated galvanized steel ducts with a nominal 3-inch diameter were used in the footing and were filled with the Polymer Concrete as a grouting material for the columns rebar dowels. The confinement of the duct cage was similar to the column and was provided by #3 spiral spaced at a 2.5-inch pitch. For comparison purposes, the embedment length of the column longitudinal reinforcement into the footing was the same as the reference columns (i.e., PNC and S1-Bond column models) and was equal to 28 in. This embedment length is corresponding to roughly $28d_b$, where d_b is the diameter of the column longitudinal reinforcement. Note that all reinforcement used was Grade 60 (either A615 or A706).

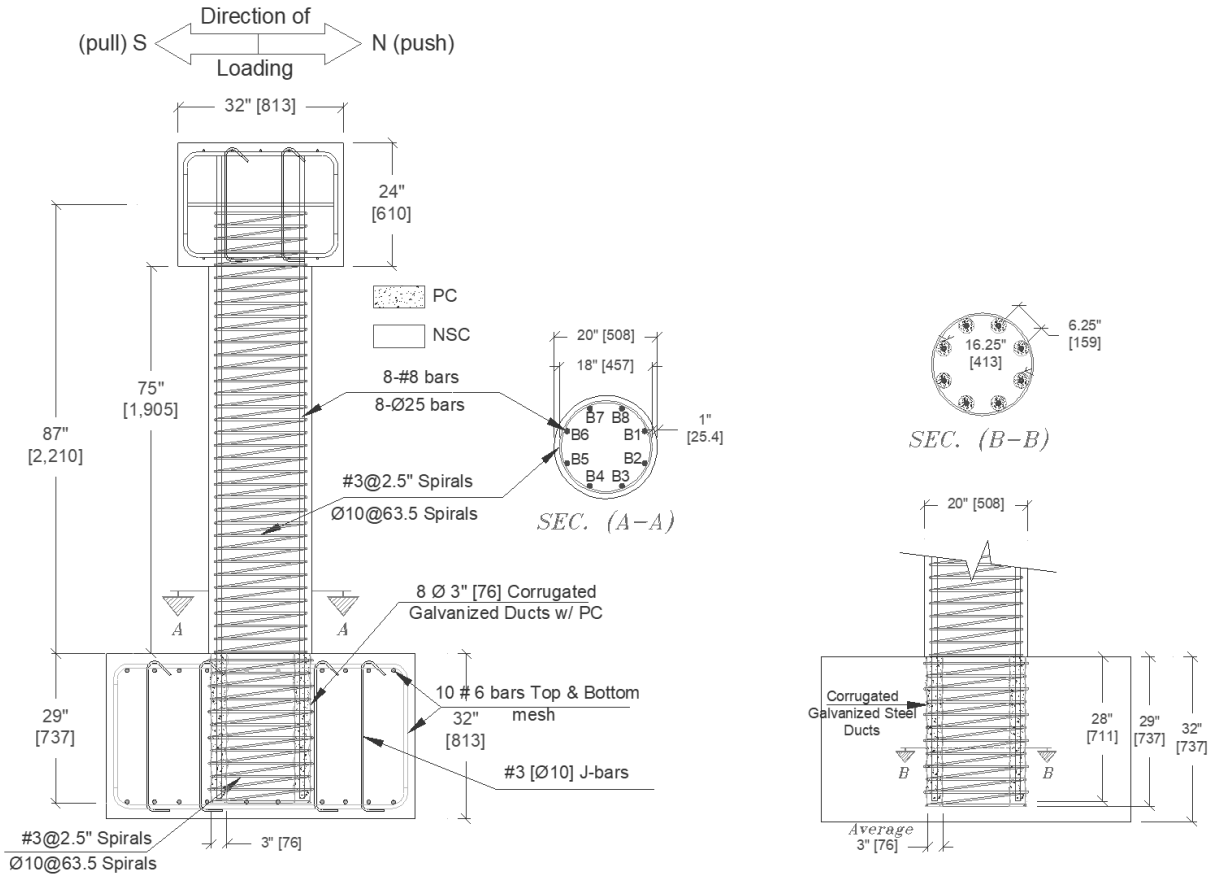

Figure 3.6 PDC Column Model.

The construction stages of the column models are illustrated in Figures 3.7 through 3.10 and they are as follows:

(1) Casting the footing with ducts (Figure 3.7).
(2) Casting the precast column with extended longitudinal bars at the column base (Figure 3.8).
(3) Filling the ducts with PC using a tremie tube method (Figure 3.9).
(4) Installing the precast column in the footing through the ducts (Figure 3.10).

To keep the corrugated ducts in their designated places during the pouring, a wooden formwork pattern was made specifically for this reason as shown in Figure 3.11. Based on the observations obtained from the reference column S1-Bond which had a soft load-drift behavior because of the irregular column-to-footing surface interface, two precaution measures have been followed to ensure the column plumbness and eliminated any imperfection at the footing surface. Firstly, after the footing concrete hardened, a grinding machine was used to remove the excess irregular

concrete parts from the surface (Figure 3.7). Secondly, an intentionally made thin bedding layer of PC is used to grout underneath the column-footing interface surface area when installing the column into the footing. A picture of the overflow is shown in Figure 3.12.

Figure 3.7 Precast Footing with Embedded Ducts.

Figure 3.8 Precast Column with Extended Longitudinal Bars.

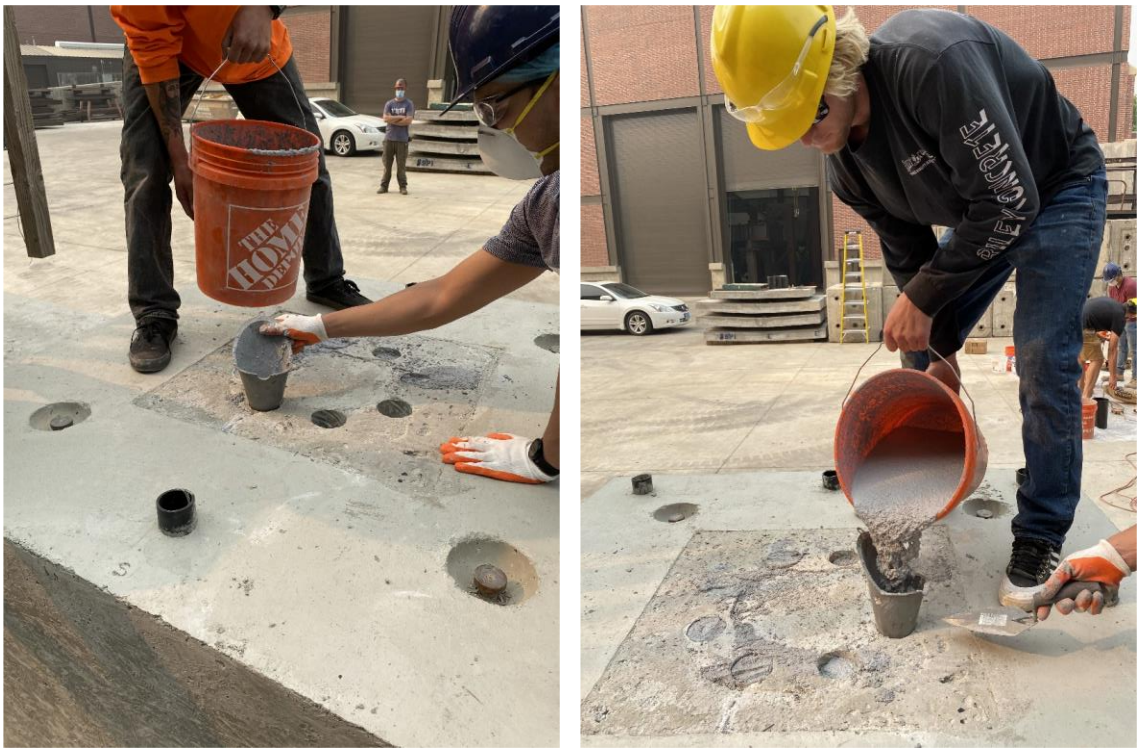

Figure 3.9 Casting UHPC into the Ducts using Tremie Tube Method.

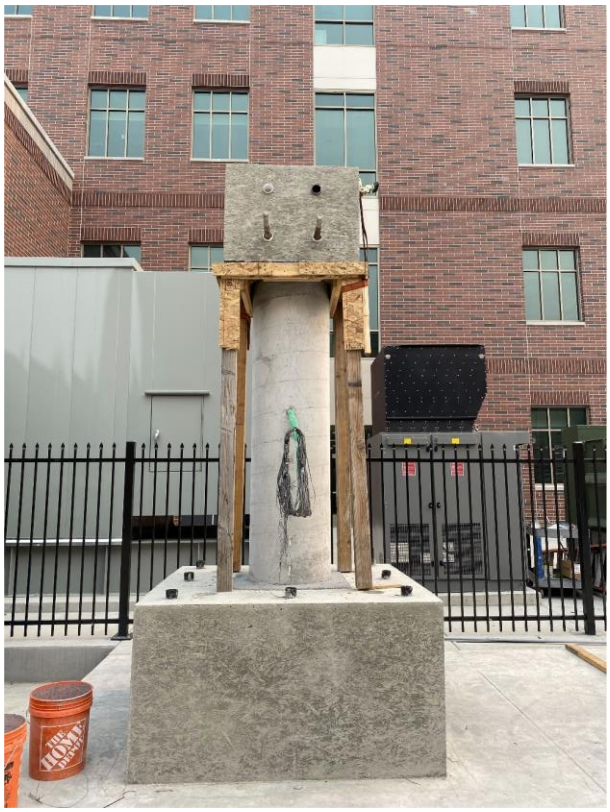

Figure 3.10 Erecting and Installing the Columns in the Footings through Ducts.

Figure 3.11 Wooden Formwork Pattern to Keep the Ducts in Place While Pouring.

Figure 3.12 A Thin Layer of PC Bedding Underneath Column-Footing Interface.

3.3. Instrumentation Plan

Global and local responses of the tested column models were measured by 16 displacement transducers and string potentiometers. Strains of the reinforcements were measured by strain gages installed at different levels. Each specimen was instrumented with 40 reinforcement strain gages distributed along six levels in the column plastic hinge region and inside the footing to capture the

longitudinal bars, and the transverse bars strains as shown in Figure 3.13. The strain gages were labelled according to their position and their height levels. The notations of "N", "S", "E" and "W" stand for North, South, East and West directions, respectively, while the numbers following those notations denote the 6 levels of the strain gages, starting from level "1" at 6-inch below the column footing interface and ending with level "6" at 21-inch above the footing surface.

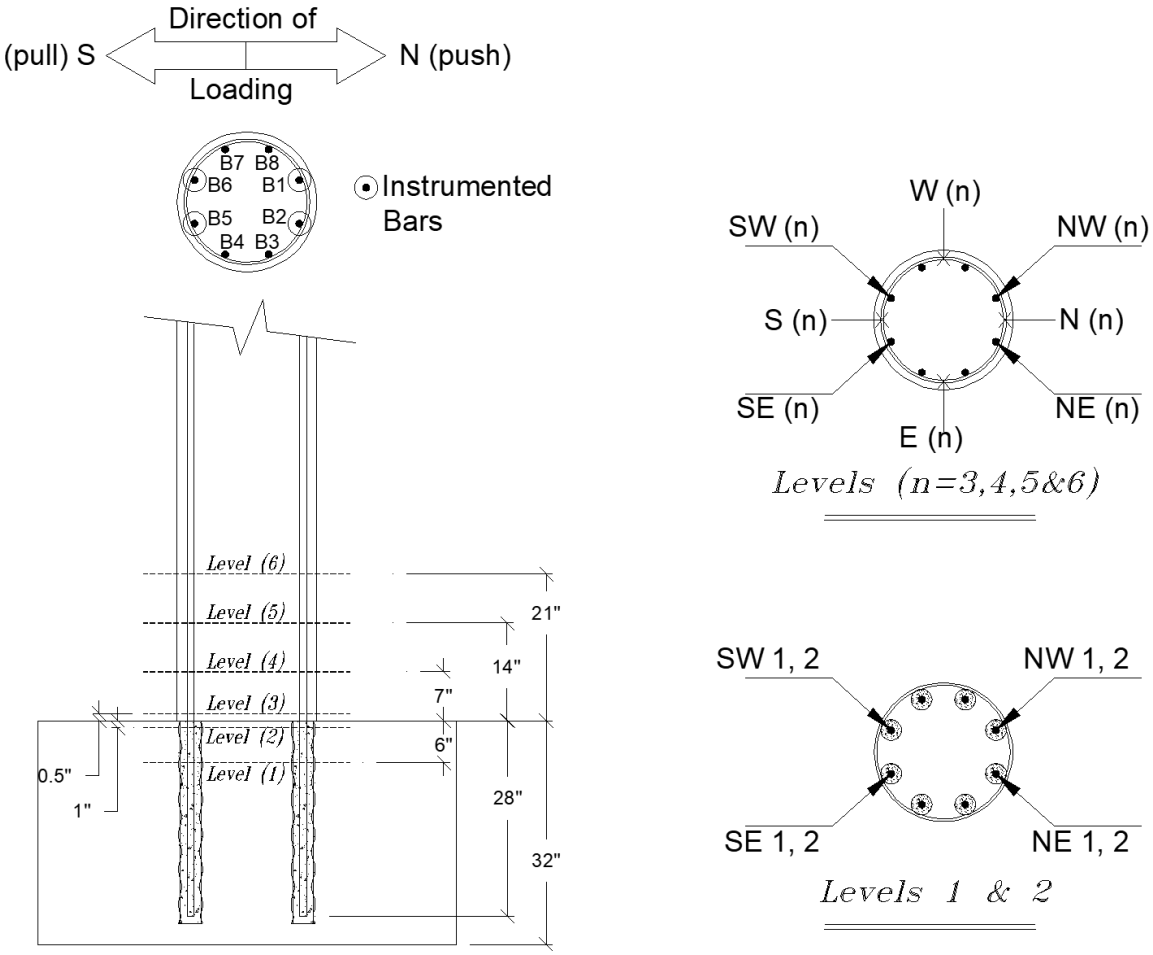

Figure 3.13 Locations of Strain Gages in PDC Column Model.

Rotations and curvatures of the columns at plastic hinges were measured by 12 vertical displacement transducers distributed onto six levels and placed at opposite faces of the columns in the loading plane as shown in Figure 3.14. The columns lateral displacements were measured by four displacement transducers (string potentiometers) installed on the column head. The applied lateral forces were measured by the actuator load cell.

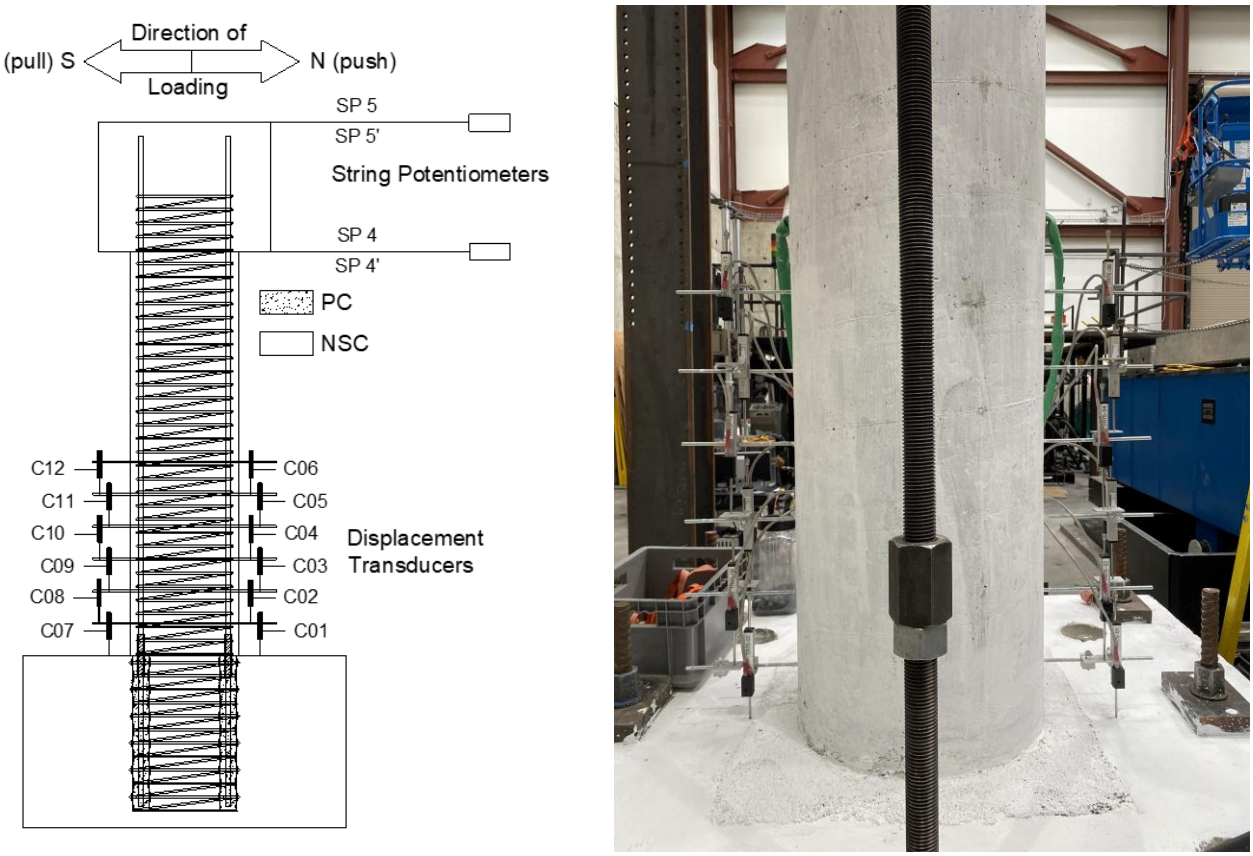

Figure 3.14 Displacement Measurement at Opposite Face of Columns in Plastic Hinge.

3.4. Test Setup and Loading Protocol

The column was tested in a cantilever configuration setup as shown in Figure 3.15. Support for the actuator was provided by mounting it on the laboratory strong wall, while the specimen was fixed to the ground through prestressed bars attached to the laboratory strong floor. A 220-kip servo-hydraulic actuator was used to apply cyclic loads to the column with displacement-controlled loading. Axial load was applied to the columns using two 200-kip hollow core jacks installed on a spreader beam perpendicular to the loading direction.

The column was subjected to a 157-kip axial load and was kept constant during test. The axial load was equivalent to an axial load index of 10% based on the design column concrete compressive strength of 5 ksi at 28 days. The axial load index is the ratio of the axial load to the product of the column gross section area and the specified compressive strength of the concrete column. The cyclic loading protocol was adopted and matched from the previously tested reference column models and is shown in Figure 3.16. Two full cycles were completed at each of the

following drift ratio levels: 0.25%, 0.5%, 0.75%, 1%, 2%, 3%, 4%, 5%, 6%, 8%, 10%, and 12%. The drift ratio is the ratio of the lateral displacement to the height of the column measured from the top of the footing to the center line of the horizontal actuator. Two displacement rates of 1 in/min and 5 in/min were used in the test. The former was used for drifts below 3.0% and was chosen to be slow enough to allow ongoing checking of strain values for the purpose of capturing the rebars yield. The latter rate was to measure the post-yield strength of the column from 3% drift to failure. The rates were based on ASTM limits for strain rates of bar tests.

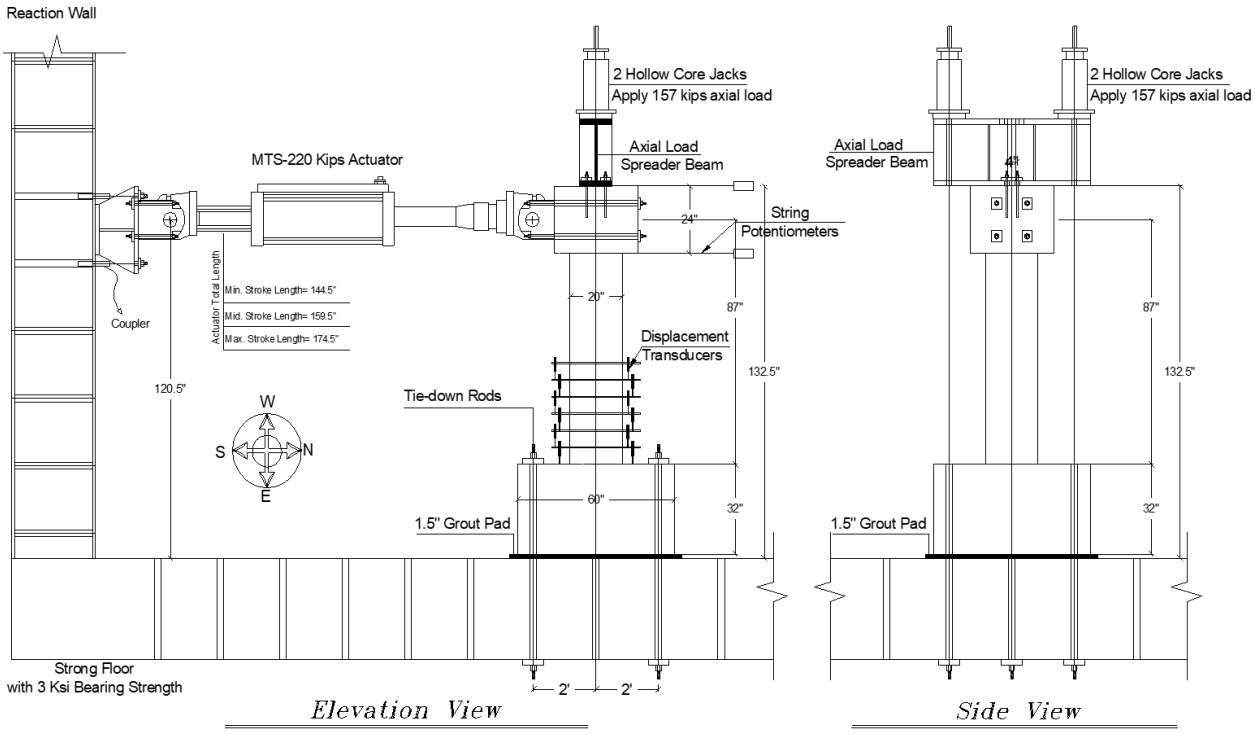

Figure 3.15 Column Test Setup under Combined Axial and Bending at UNR.

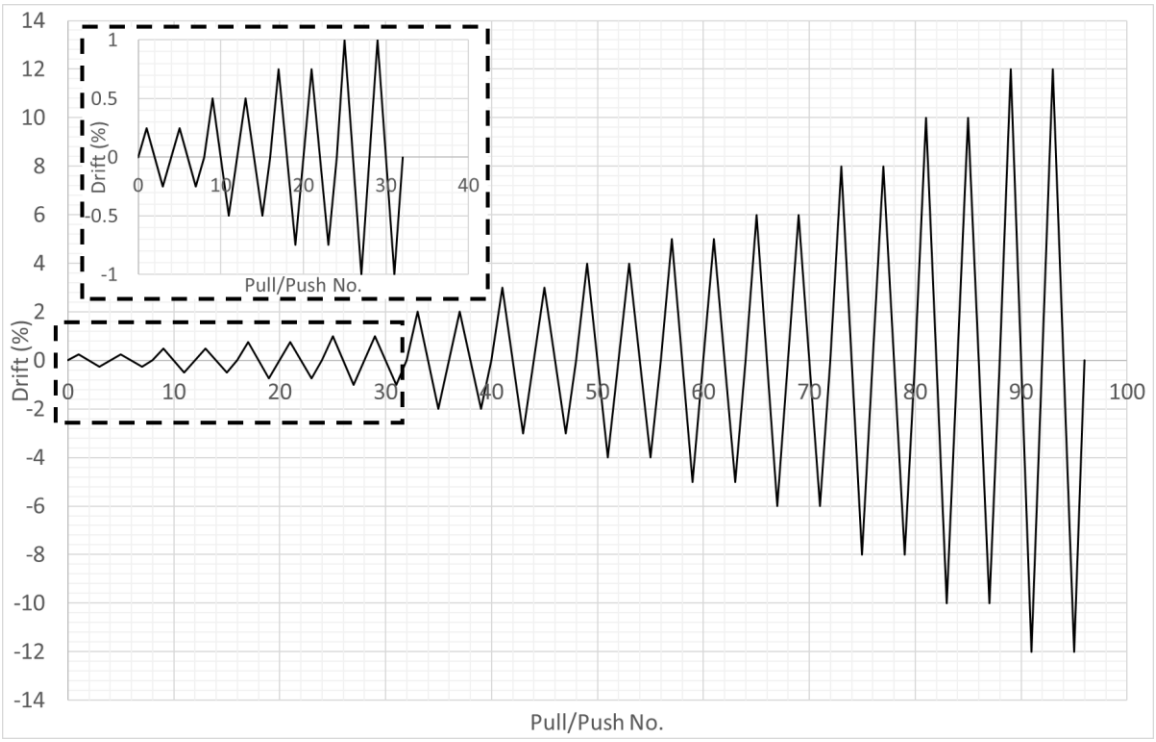

Figure 3.16 Cyclic Loading Protocol for Lateral Loading of the PDC Column Model.

CHAPTER 4. TEST RESULTS AND DISCUSSION

4.1. Introduction

This chapter presents the experimental test results of the PDC column with respect to its global and the local behavior perspectives. The test results include observed plastic hinge damage, force-displacement relationships, energy dissipation, residual drifts, strain profiles, curvature profiles, and moment-rotation relationships.

4.2. Columns Global Behavior

4.2.1. Plastic Hinge Damage and Mode of Failure

The column cross-section orientation and its longitudinal bars labeling were previously shown in Figure 3.5. The column was loaded in the North-South direction. The push load was defined as the loading of the column from south to north while the pull load was designated to the loading from the north to south (Figure 3.14). The damage sequence of the column up to failure was as follows: concrete flexural cracks, significant concrete cover spalling, longitudinal bars buckling, spirals fracture, concrete core spalling and finally longitudinal bars fracture at the column-footing interface during the 10% and 12% drift cycles. Using only evidence from visual inspection and surface damage, it can be implied that no damage of the PC-filled duct connection such as bar pullout, duct pullout, or concrete breakout failure of the footing took place. In previous studies (e.g. Subedi et al. 2019), such modes of failure like duct pullout or bar pullout will propagate damage to the surface and can be seen visually at the footing top, which was not observed in this test and PC-filled connection.

The column flexural cracks were observed to start during the 0.5% drift cycles and minor shear cracks were observed during the 2% drift cycles. The column had its first bar yielding at bar B5 at 1.23% drift ratio during the 2% drift cycle at 19.75 kips lateral load. The initiation of the concrete cover spalling was observed on the North and South sides of the column during the 3% drift cycle while complete cover spalling and rebars exposure were observed during the 6% drift cycles. The buckling of the longitudinal bars was initiated in the 8% drift cycles while the severe bar buckling was observed at the 10% drift ratio. The first and second bar fractures were observed to happen simultaneously on the north side of the column during the second cycle of 10% drift then the spirals fractured on the same side of the column. Afterwards, at 12% drift cycle, the bars

on the other side of the column, i.e., south side, had significant buckling over multiple successive spirals. The combination of the bars fracture as well as the bars significant buckling and spirals fractures has led to at least 50% loss in the column lateral load capacity. Thus, the column test was stopped as further loading of the column would be meaningless after the column had already reached its drift capacity. The column drift capacity is identified here as the drift percent corresponding to 20% loss in the column lateral capacity. Figures 4.1 through 4.10 show the progression of damage at the plastic hinge region of the column at selected different drift ratios for specimen S1-Bond.

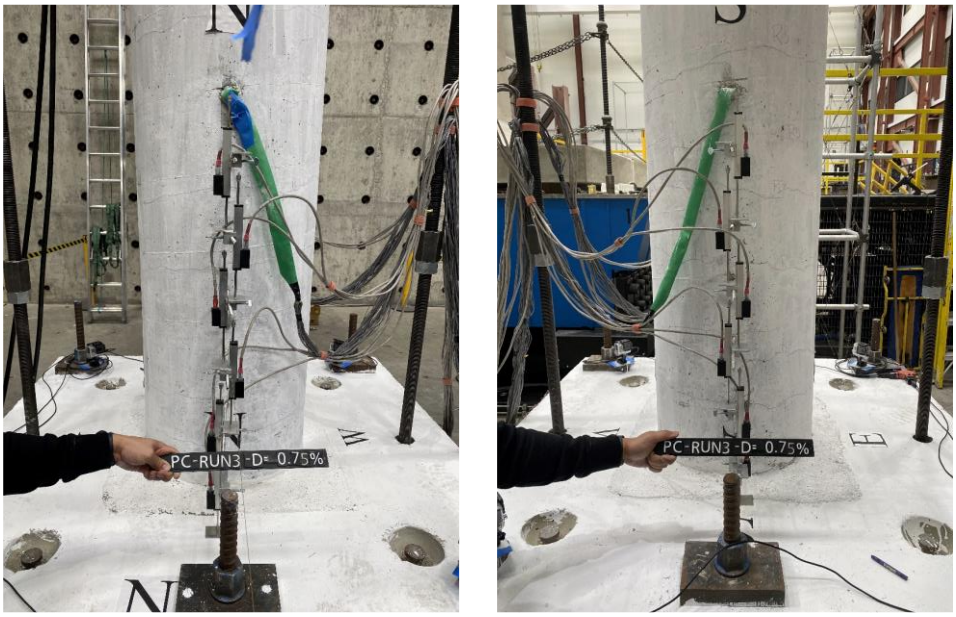

(a) North Side (b) South Side

Figure 4.1 Plastic Hinge Damage at 0.75% Drift Cycle.

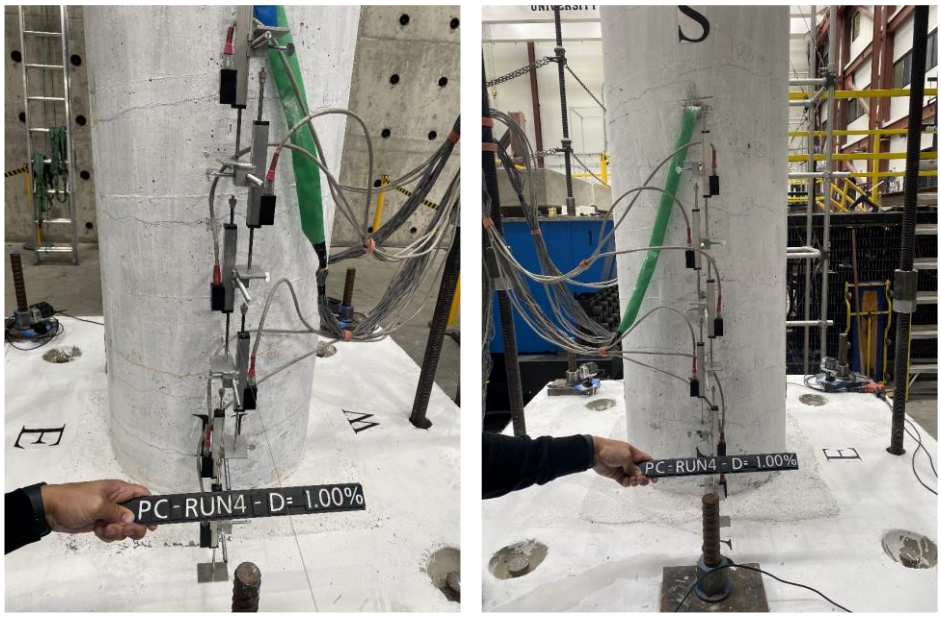

(a) North Side (b) South Side

Figure 4.2 Plastic Hinge Damage at 1% Drift Cycle.

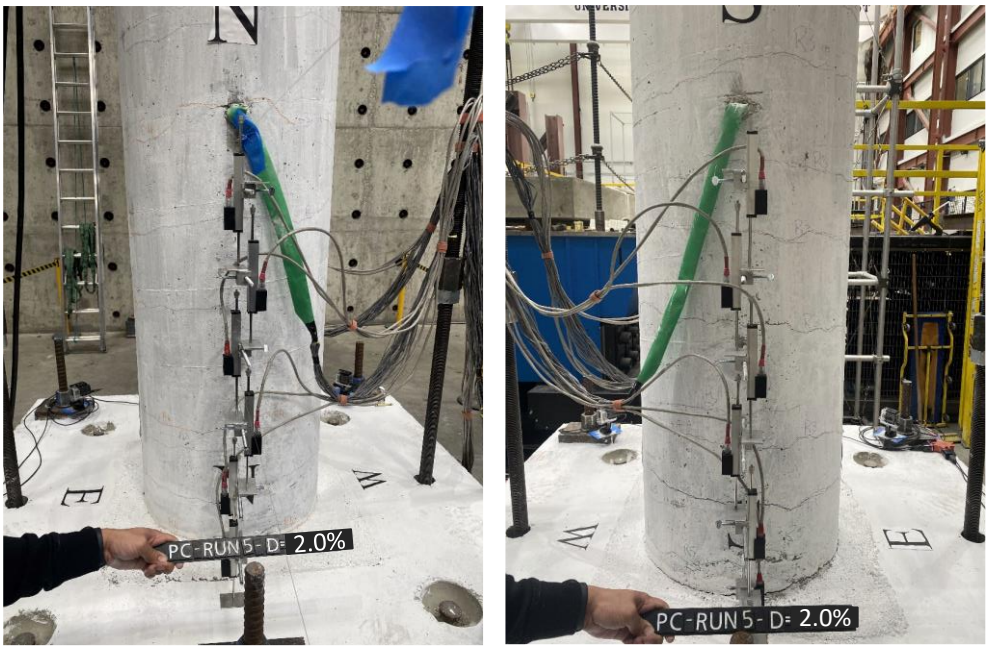

(a) North Side (b) South Side

Figure 4.3 Plastic Hinge Damage at 2% Drift Cycle.

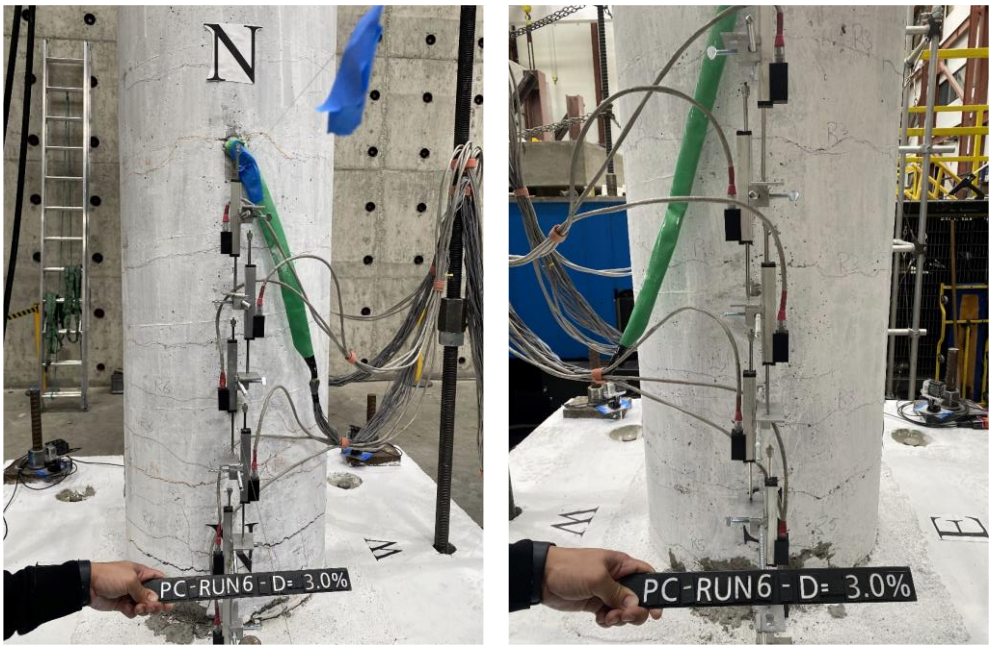

(a) North Side (b) South Side

Figure 4.4 Plastic Hinge Damage at 3% Drift Cycle.

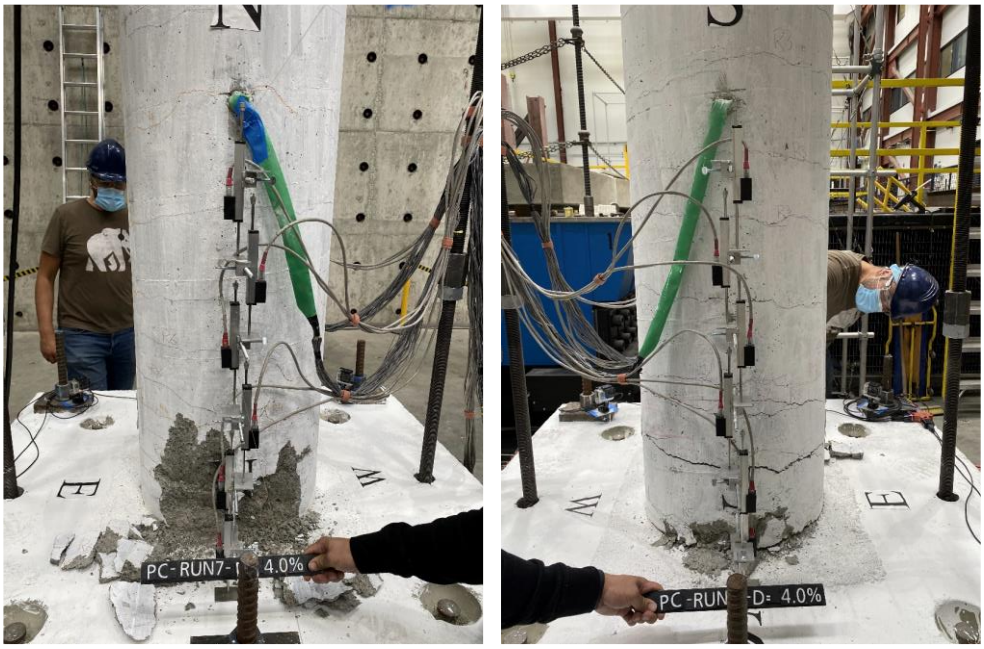

(a) North Side (b) South Side

Figure 4.5 Plastic Hinge Damage at 4% Drift Cycle.

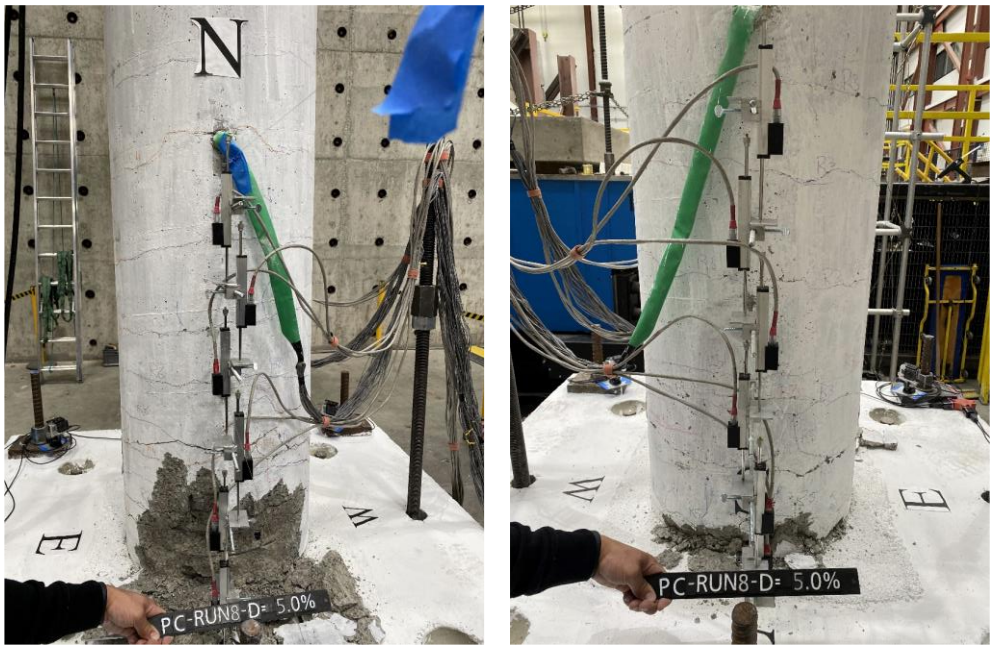

(a) North Side (b) South Side

Figure 4.6 Plastic Hinge Damage at 5% Drift Cycle.

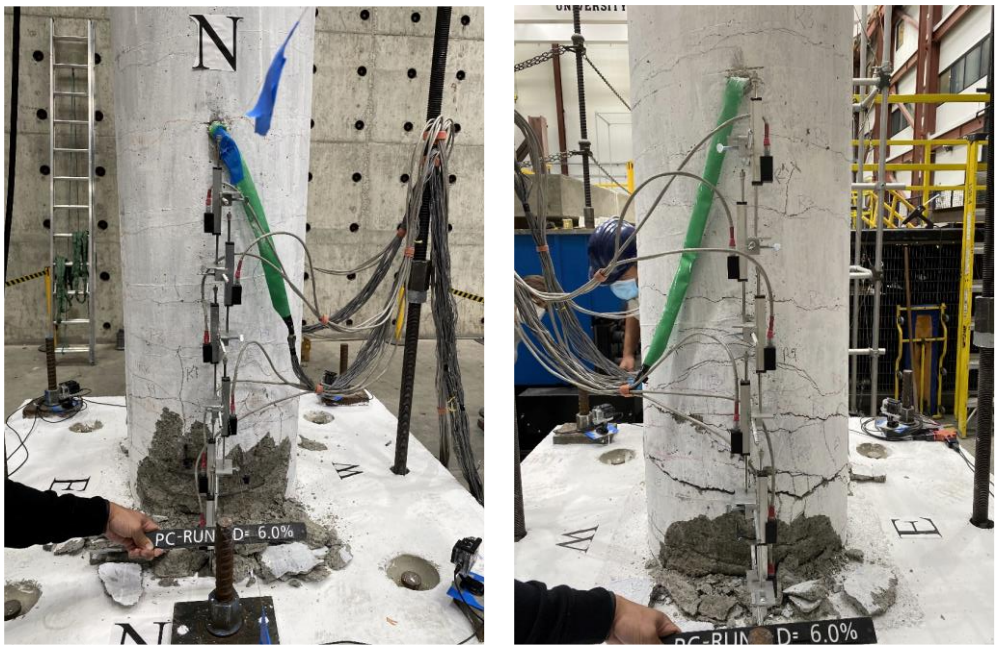

(a) North Side (b) South Side

Figure 4.7 Plastic Hinge Damage at 6% Drift Cycle.

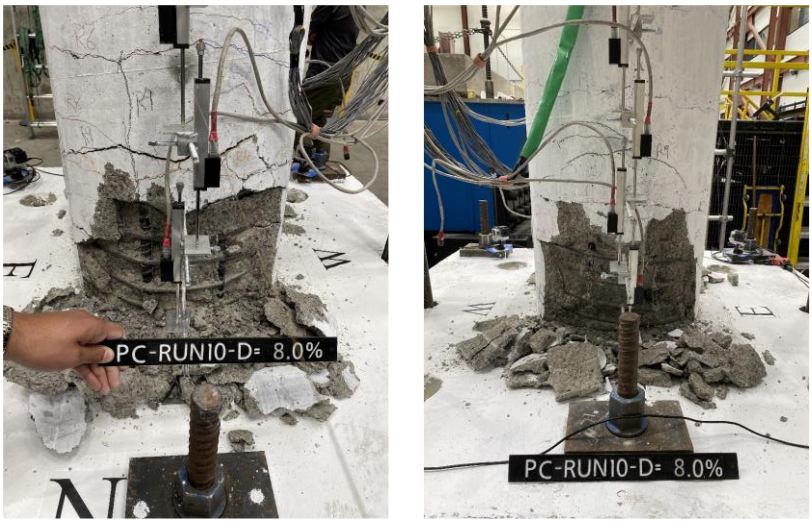

(a) North Side (b) South Side

Figure 4.8 Plastic Hinge Damage at 8% Drift Cycle.

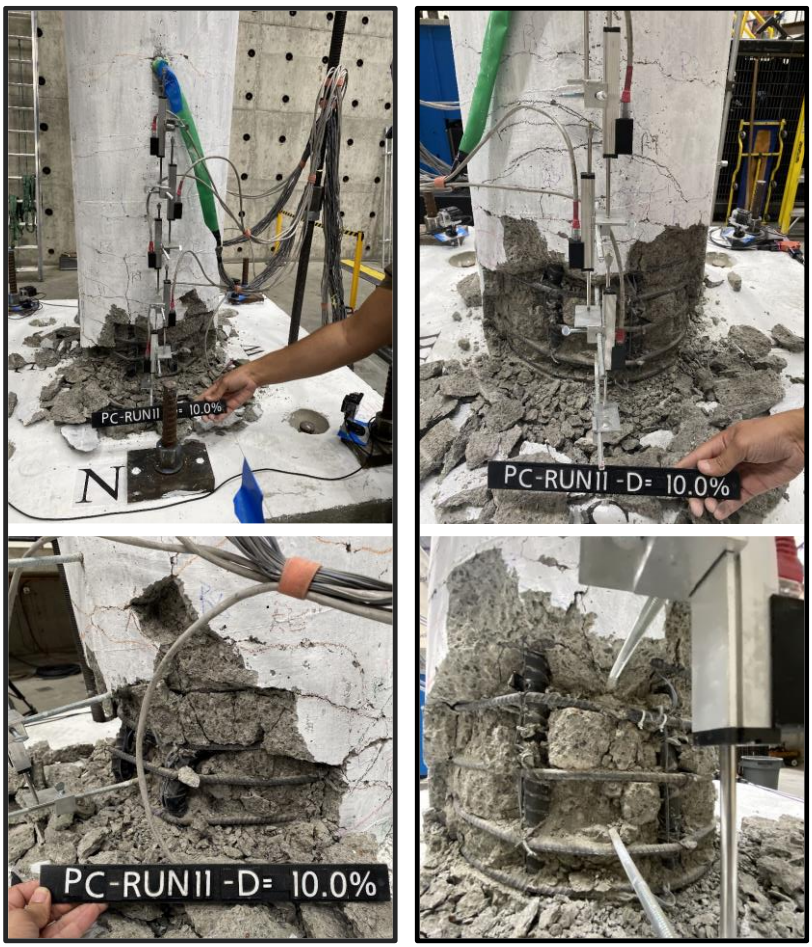

(a) North Side (b) South Side

Figure 4.9 Plastic Hinge Damage at 10% Drift Cycle.

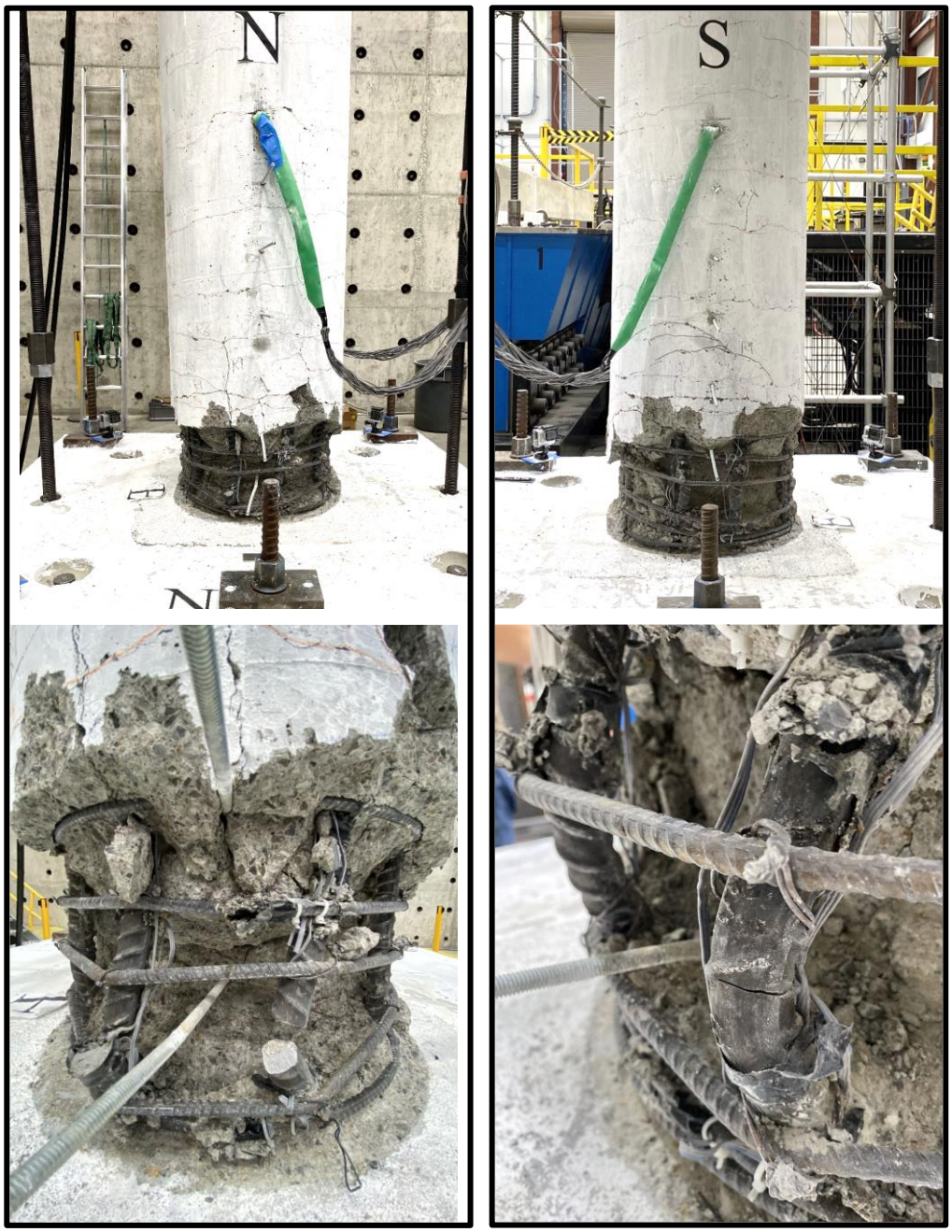

(a) North Side (b) South Side

Figure 4.10 Plastic Hinge Damage at 12% Drift Cycle.

4.2.2. Force-Displacement relationship

The measured lateral force-drift hysteretic relationship of the PDC column is shown in Figure 4.11. The sequence of bars rupture is also illustrated in Figure 4.11. The backbone envelope of the column hysteretic response in the push and pull directions is shown in Figure 4.12, while their

average response is shown in Figure 4.13. The envelopes are shown up to 80% of the push/pull base shear capacity. The PDC column did not exhibit any strength degradation up to 8% drift ratio neither in the push nor in the pull direction. However, significant strength and stiffness loss was observed during the following cycles due to the excessive bars buckling followed by successive bars and spirals ruptures. The column exhibited an almost symmetrical response for the push and pull directions with regards to the initial stiffness and ductility. However, the column exhibited a slightly higher load capacity in the pull direction than the push direction with measured lateral load capacities of 54 kips and 49.9 kips, respectively. The longitudinal bar yielded in the push direction at 1.234% drift ratio under a 42.3 kips force. The bar yielded in the pull direction at −0.97% drift ratio under a −35.8 kips force.

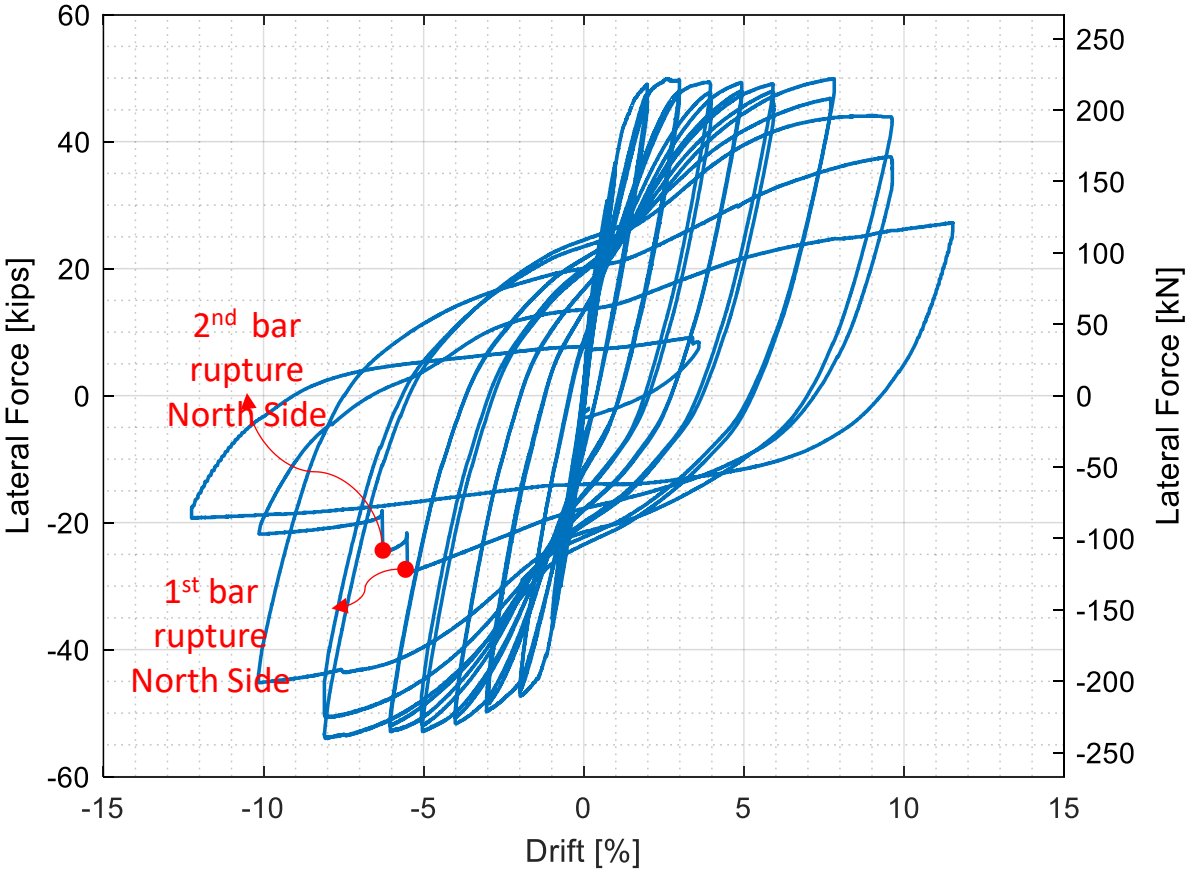

Figure 4.11 PDC Column Force-Drift Hysteretic Response.

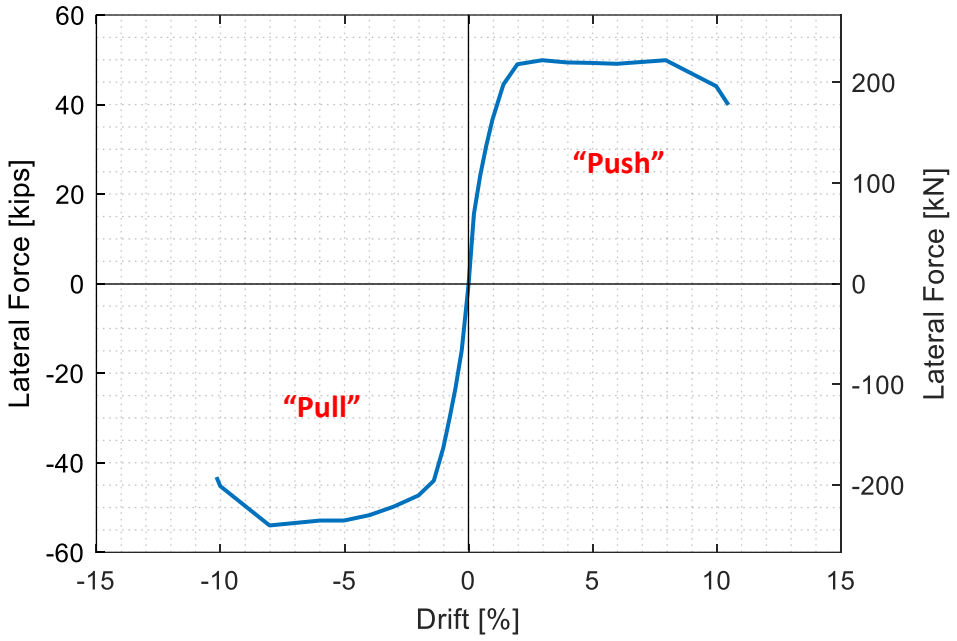

Figure 4.12 PDC Column Push/Pull Force-Drift Backbone Envelopes.

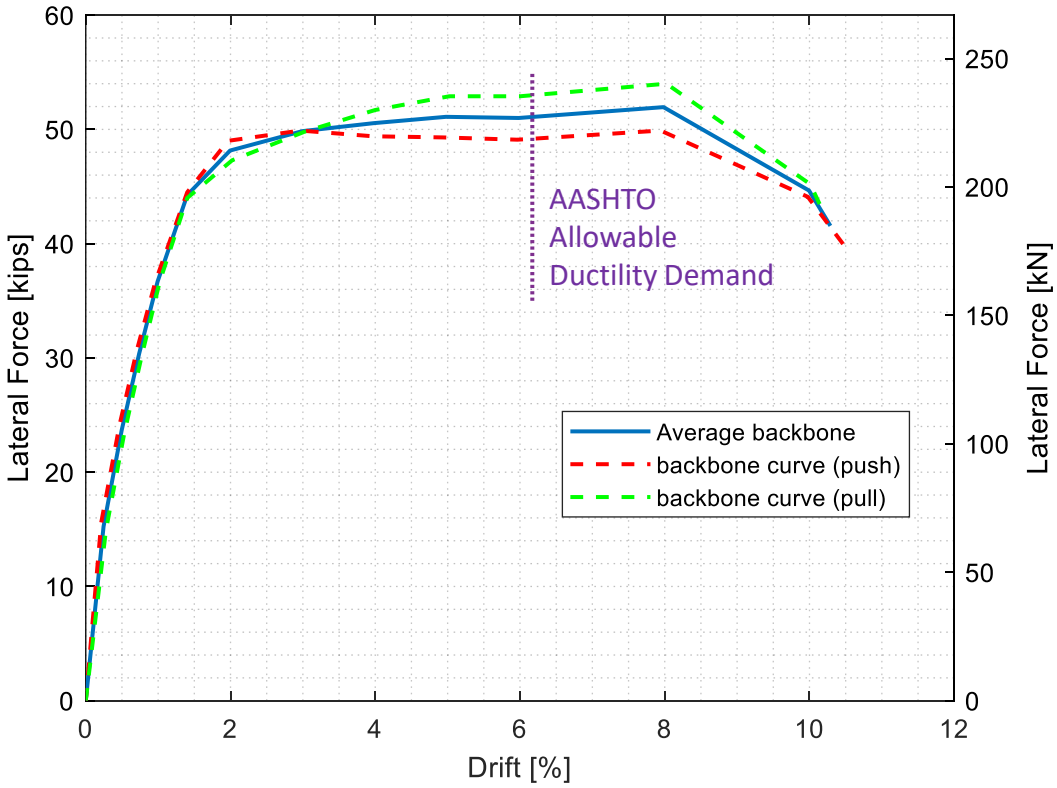

Figure 4.13 PDC Column Average Push/Pull Force-Drift Envelope.

Displacement ductility is considered to be a good representation for the ability of a column member to undergo post-yield displacements. For this study, the displacement ductility was determined by idealizing the force-displacement average envelope with an elastoplastic bi-linear curve as illustrated in Figure 4.14. The slope of the elastic branch is adjusted such that the curve begins at the origin and passes through the measured first longitudinal bar yield point. The plastic branch is set to have equal areas enclosed above and below the bi-linear plastic branch and the actual force displacement curve. The effective yield displacement $\Delta_{y,Eff}$ is defined as the displacement corresponding to the point of intersection between the elastic and plastic curves. Also for this study, the column drift capacity is determined when the column lateral load capacity drops to 80% of its peak strength due to either bar rupture or the column core concrete crushing. Hence, the ultimate displacement is determined at this point. The displacement ductility is defined as the ratio of the ultimate displacement to the effective yield displacement.

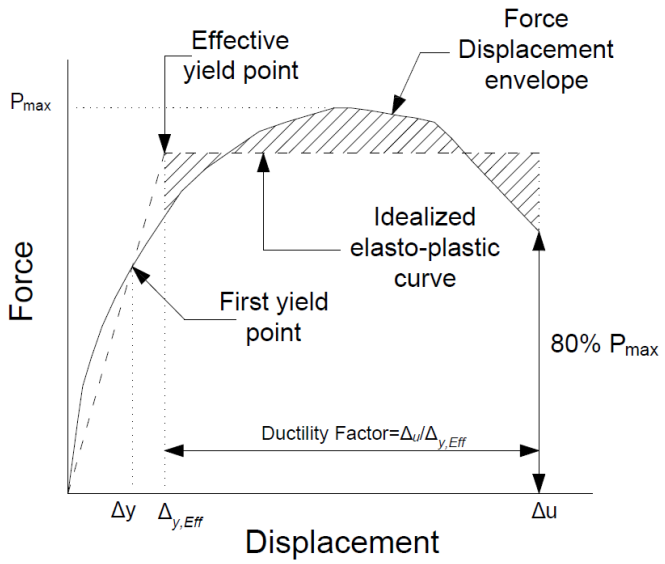

Figure 4.14 Illustration of displacement ductility calculation using elastoplastic response.

The measured average drift ratios corresponding to the first yield for the PDC column was 1.234%. Meanwhile, the effective yield drift ratios were estimated based on the procedure in Figure 4.14 to be 1.44% and its measured ultimate drift ratios was 10.29%. Accordingly, the measured displacement ductility for the PDC column was almost 7.13. It is noted that this column has met and exceeded the AASHTO (2014) requirements for maximum displacement ductility demand of 5.0. The equivalent drift ratio at the corresponding ductility of 5 is indicated in Figure

4.13, which confirms the acceptable seismic response of the column. It is also observed from Figures 4.13 that the PDC column had more than 66% reserve displacement capacity, when compared to AASHTO demand. This adequate displacement capacity allows the columns incorporating the polymer filled duct connection to be used in high seismic regions. The reserve displacement capacity was estimated as the percent increase of the column displacement capacity more than the column displacement demand corresponding to the displacement ductility demand of 5.

4.2.3. Residual Displacements

The residual displacement is defined as the displacement at which the unloading force-displacement curve intersect with the abscissa. The residual drift is the ratio of the residual displacement to the column height as measured from the footing surface to the loading point, which was measured to be 87 in [2.21 m]. Figure 4.15 shows the relation between the average residual drifts of the push and pull directions and their corresponding peak drift cycles for the PDC column model.

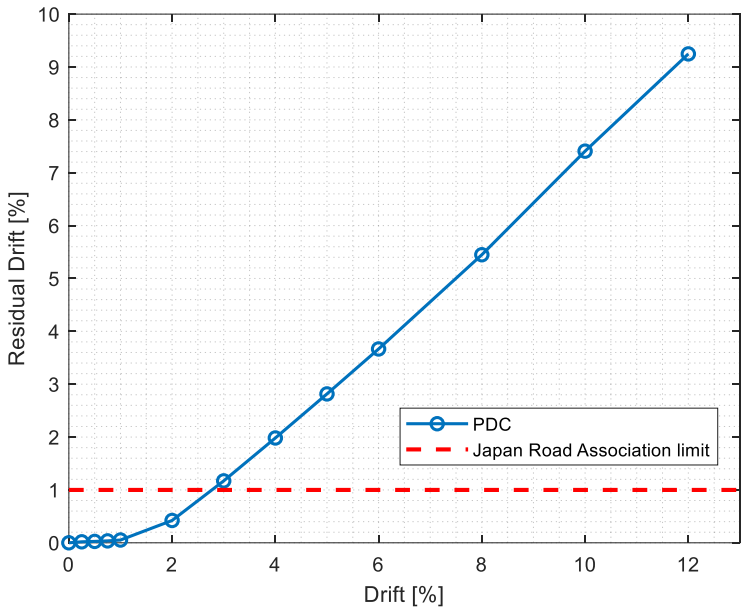

Figure 4.15 Measured residual drifts of PDC column model

No limits have been specified by any of the US bridge design codes on the residual drifts of columns for different seismic hazard levels. However, a performance criterion was found in the Japanese seismic design specifications for highway bridges 2002, which specified a 1% limit as an acceptable residual drift to open bridges for traffic after seismic events. As shown in Figure

4.15, the PDC column has met the 1% residual drift limit at approximately 2.8% drift ratio, which is roughly equivalent to quarter the average drift capacity of both columns. This result is comparable to the benchmark column models (CIP, PNC and S1-Bond), where the benchmark columns have met this criterion at approximately 3% drift ratio. While the 2.8% or 3% values are not assessed against a specific seismic hazard level, the comparison provides another evidence that polymer concrete filled duct connection is acceptable and emulative.

4.2.4. Energy Dissipation

The cumulative dissipated energy of PDC column is shown in Figure 4.15 at different drift levels. The energy dissipation of the column is measured by integrating the area enclosed between the lateral force-displacement response and the abscissa. It can be seen that the PDC column exhibited a good energy dissipation response that is consistent with the force-displacement response as well as the damage progression observations. The column kept an exponential cumulative energy dissipation response at the first few drift cycles up to approximately 4% drift, then kept almost constant increasing rate up to 10%, then finally, the cumulative response switched to a downgrade behavior as the column had its failure in the form of bars rupture and complete cover spalling. This dissipated energy response was very similar to the typical response of the CIP columns with monolithic connections to their footings.

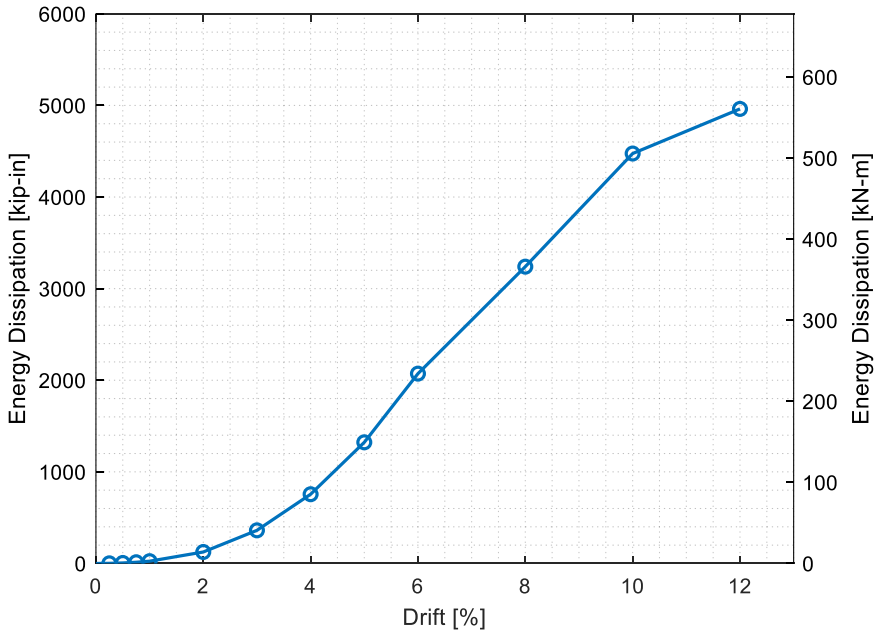

Figure 4.16 Cumulative Energy Dissipation for PDC Column.

4.3. Columns Local Behavior

4.3.1. Strain Profiles

The PDC column was comprehensively instrumented with a total of 40 reinforcement strain gages placed onto six levels along the column anticipated plastic hinge zone and inside the footing to measure the strains of the longitudinal reinforcement and transverse spirals (see Figure 3.12 above). The maximum tensile strains measured at the different drift ratios are shown Figure 4.16. The instrumented bars were B1, B2, B5, and B6 which are the North-East, North-West, South-East and South-West bars, respectively. It is worth mentioning that most of the strain gages near the column-footing interface were damaged as the column approached its drift capacity. Thus, the strain gages readings were only reported in Figure 4.16 up to their damage. The largest recorded reinforcement strains were at levels 2 and 3 (ie., 1 in. below and above the column-footing interface, respectively). This observation confirmed that the reinforcing bars had full development into the footing and were emulative to the plastic hinge behavior to a typical CIP column.

The longitudinal reinforcement strain profiles are shown in Figures 4.17 to 4.18 for the lower drift ratios up to 3%, and for higher drift ratios above 3%, respectively. The strain profiles shown in the figure are the maximum measured tensile strains of bars B1, B2, B5 and B6 at the different heights of the column. The strain profiles were almost uniform along the column height prior to bar yielding. However, strains started to exponentially increase near to the column-footing interface at and above 2% drift ratio at which strains exceeded the yield strain significantly.

The spirals strain profiles at the North, South, East and West sides of the PDC column are shown in Figure 4.19. Almost all spirals remained elastic and had uniform distribution up to 8% drift ratio and they increased afterwards due to the initiation of bars buckling. Comparing the spirals strains at the North and South sides to those in the East and West sides, it is obvious that the latter had more strains, which is a typical observation for the transverse reinforcement strains perpendicular to the bending moment direction.

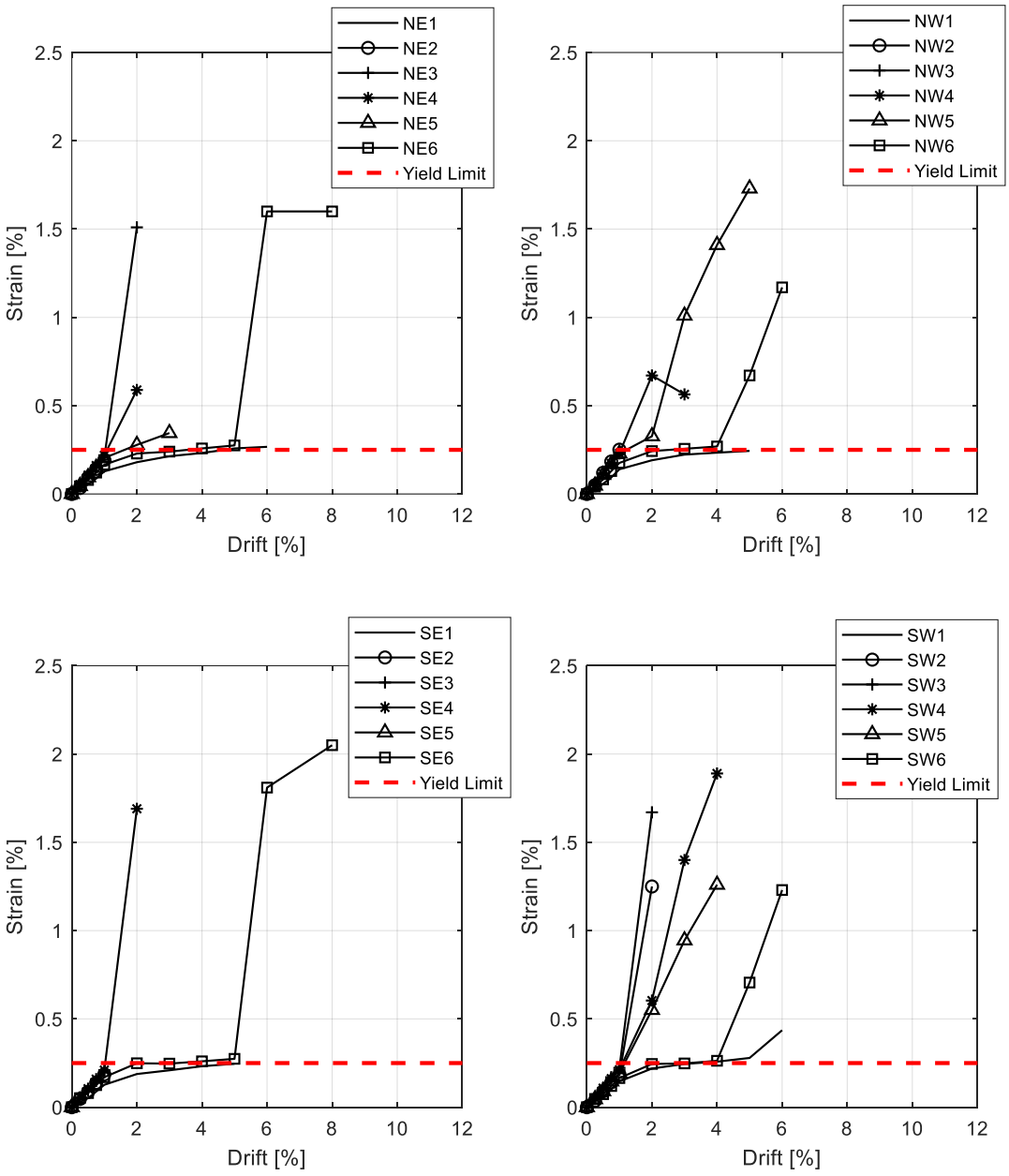

Figure 4.17 PDC Column Strains versus Drift Ratio.

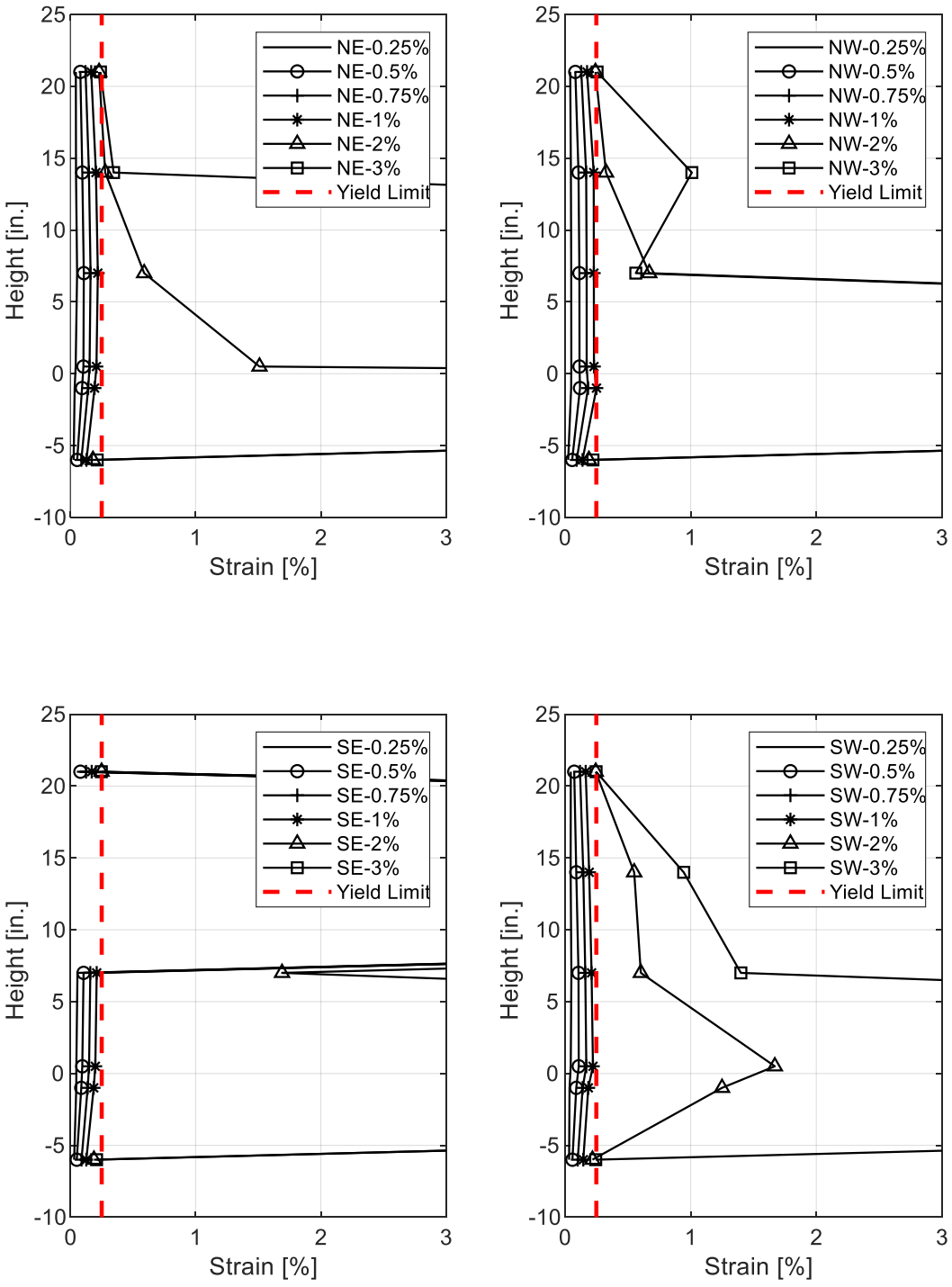

Figure 4.18 Strain Profile for Longitudinal bars of PDC Column for Lower Drift Ratios.

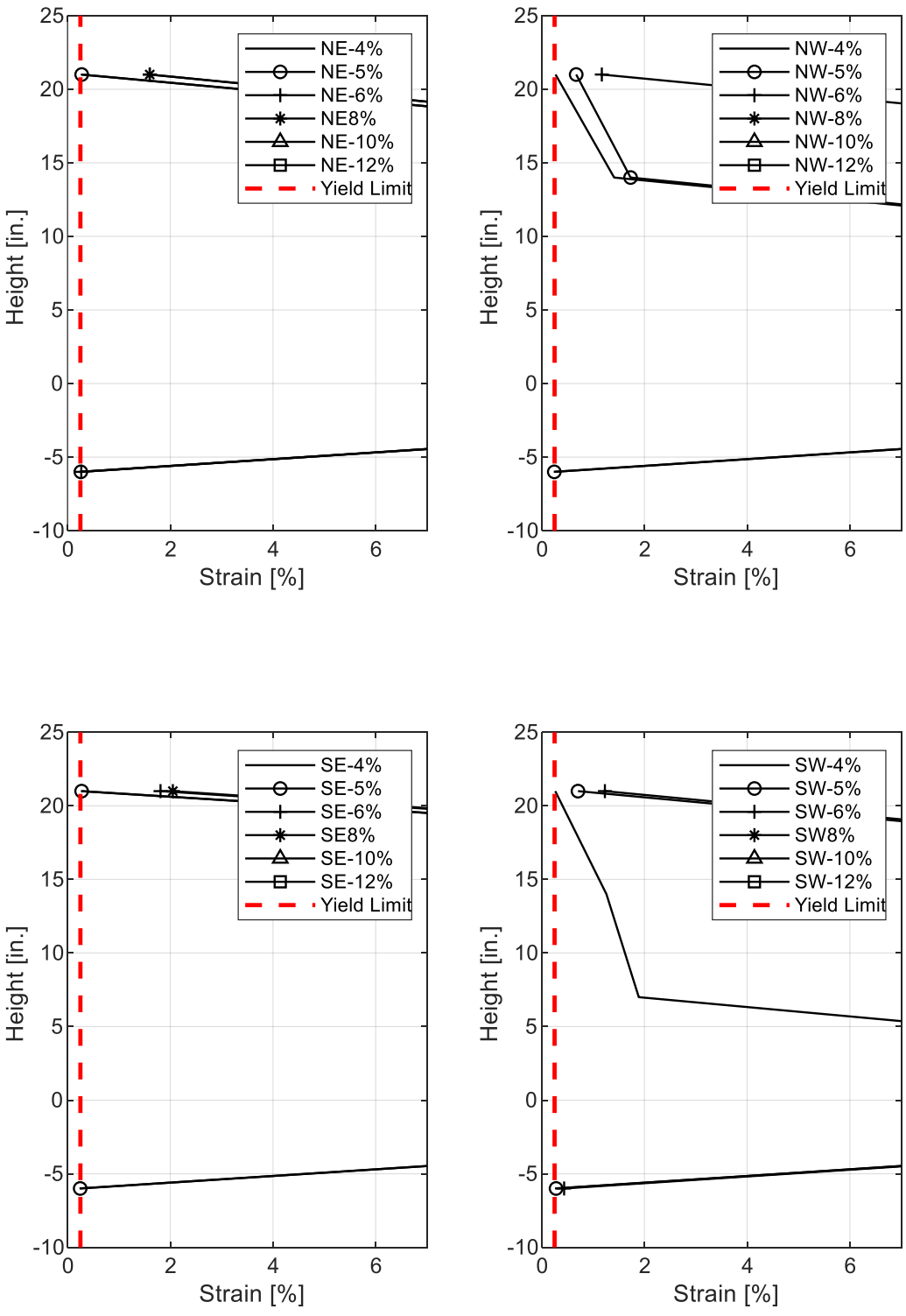

Figure 4.19 Strain Profile for Longitudinal bars of PDC Column for Higher Drift Ratios.

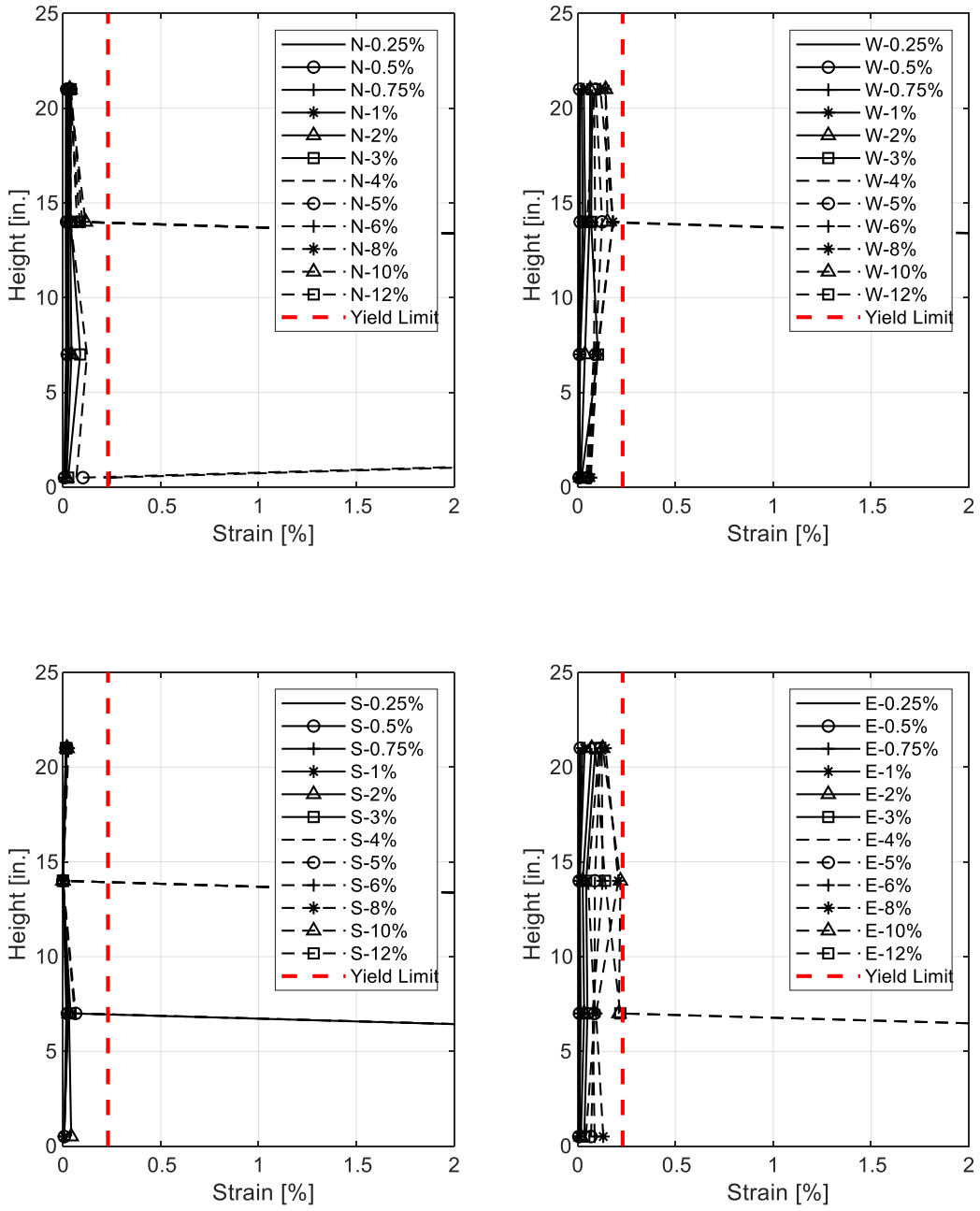

Figure 4.20 Strain Profile for Spirals of PDC Column.

4.3.2. Curvature Profiles

The curvature profiles of the plastic hinge region reported at the different drift levels are shown in Figure 4.20. Curvatures were measured indirectly by using displacement transducers mounted on both loading sides of the columns as illustrated before in Figure 3.13. Curvatures at each level were computed as the ratio of the section rotations of that level to the vertical distance of the

transducers. The rotations were, in turn, the ratio of the summation of the relative displacements to the horizontal distance between the transducers in the same level. The curvature was measured at six levels. The curvature of the column at the base, i.e. footing interface, was the highest mainly because of yield penetration at the column-footing interface. This confirms that the PDC column was able to emulate the plastic hinge behavior of a CIP column. It is worth noting that the displacement transducers at the column-footing interface became inoperative at the higher drift ratios loading cycles beyond 8% as they reached their maximum stroke.

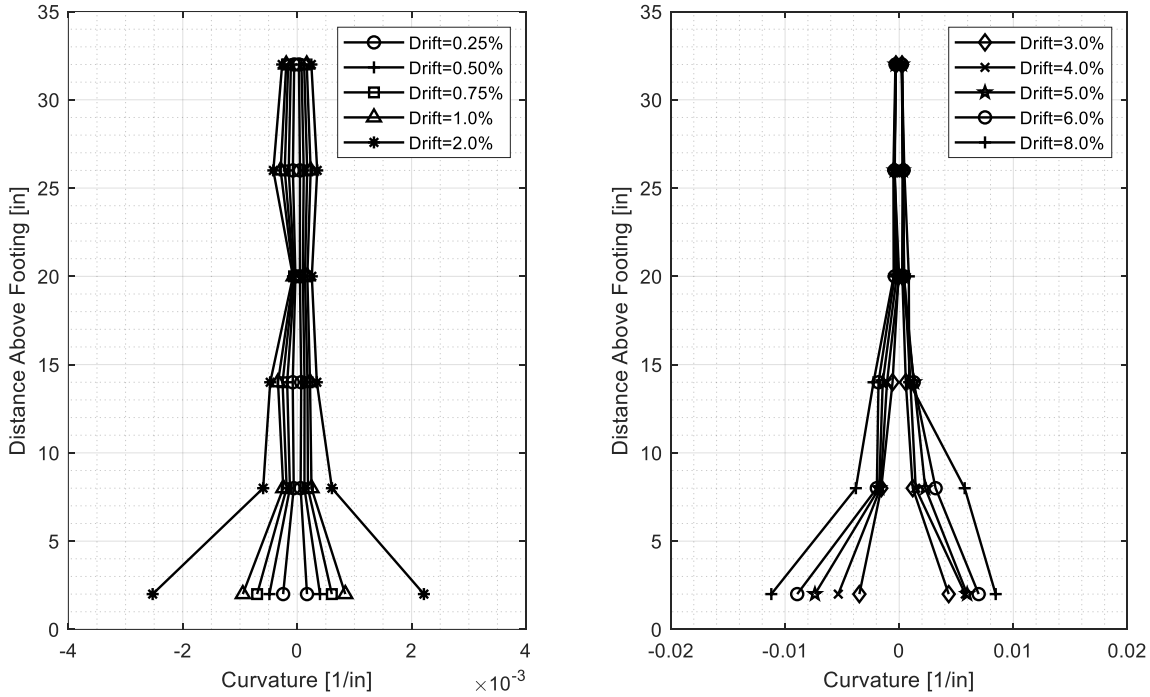

Figure 4.21 Curvature Profile of PDC Column.

4.3.3. Moment-Curvature Behavior

The measured base moment-rotation relationship (closest level to the footing) of the PDC column is shown in Figure 4.22. The corresponding base moment-drift relationship is also shown in Figure 4.23. The behavior implied through the figures is the same explained above using force-drift relationships. Nevertheless, the maximum moment capacities can be reported from the figures in this section in the push and pull loading sides for the PDC column as 4,341 kip-in and 4,698 kip-in, respectively.

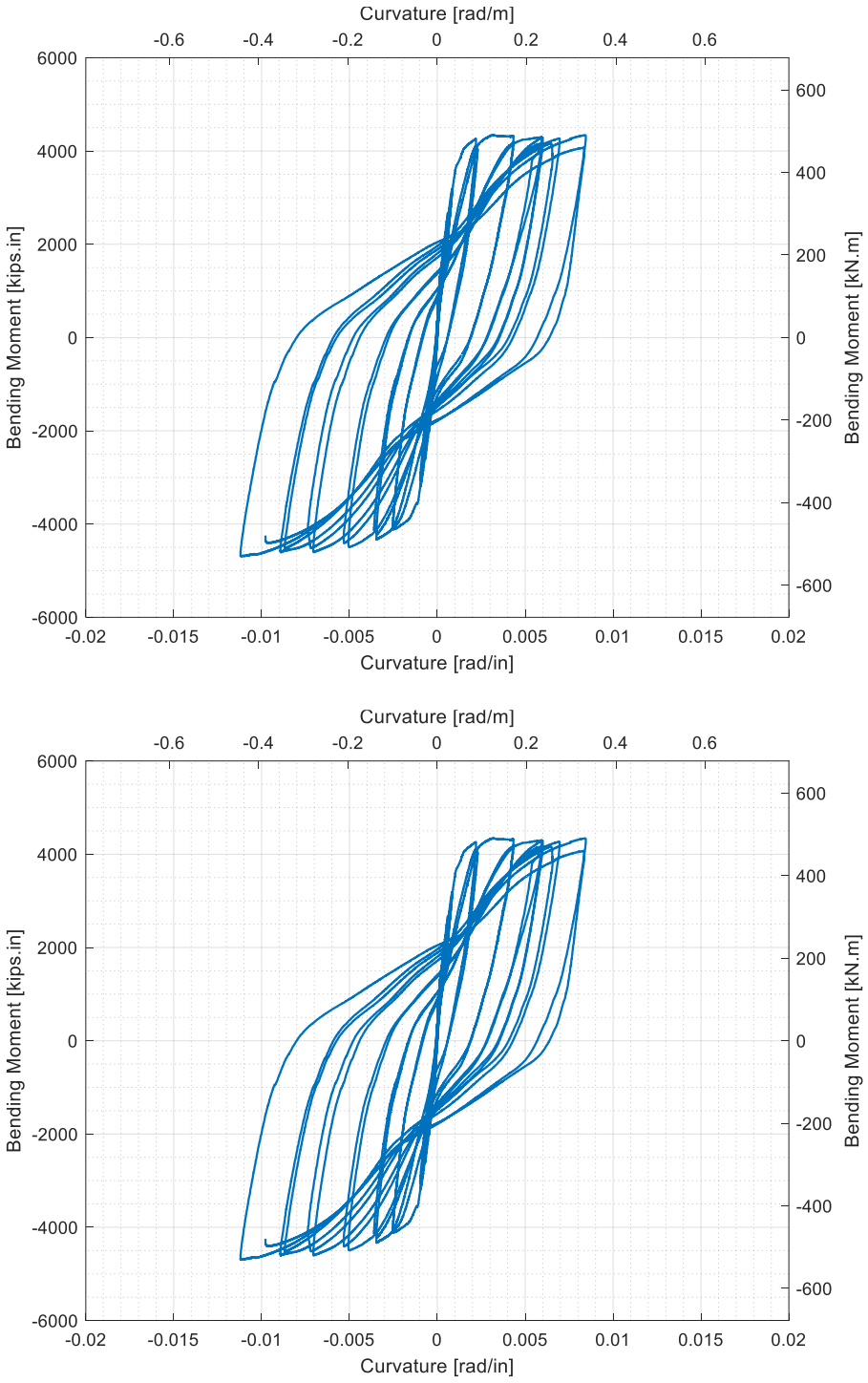

Figure 4.22 Moment-Curvature Hysteretic Behavior of PDC Column at 2 in above column-footing interface.

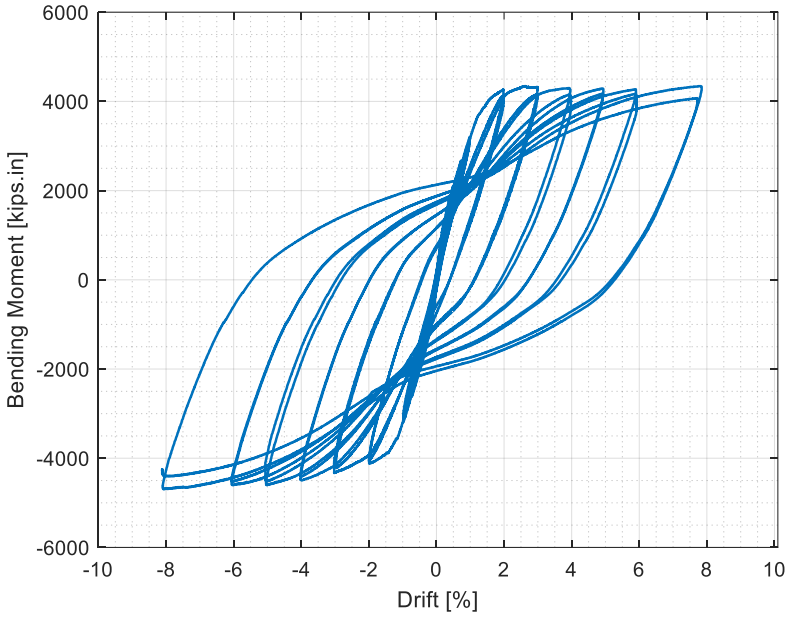

Figure 4.23 Moment-Drift Hysteretic Behavior of PDC Column.

4.4. Column Models Evaluation with Respect to Previous Studies

The chapter also provides a normalized comparison with the three previous columns tested at UNR as found in the literature, i.e. CIP, PNC, and S1-Bond columns. The test results of the column model tested in this study, i.e. PDC column, was independently and comprehensively presented in the previous sections. In this section, the overall seismic performance of this column is further assessed and compared with a reference CIP column tested by Haber et al. (2013) as well as another PNC column model with ducts filled with proprietary UHPC tested by Tazarv and Saiidi (2014) and finally with the S1-Bond column model which had non-proprietary UHPC filled duct connection by Aboukifa et al. (2021). The summary of the different column models design was previously shown in Table 3.1. The so-called PNC model was a precast column model that had its longitudinal bars extended into a proprietary UHPC-filled duct placed in the footing while the S1-Bond column models had their bars extended into non- proprietary UHPC-filled ducts inside the footing. It is noted that all columns used Grade 60 reinforcing steel, so there should not be differences in the behavior associated with varying reinforcement.

All the column models experienced the same mode of failure as it started with concrete cover spalling followed by longitudinal bar buckling and then finally bar fracture. No damage of the UHPC-filled duct connection such as bar pullout, duct pullout, or conical failure of the footing

concrete was observed in either of the UHPC-filled ducts or the PC-filled ducts column models. The PNC column withstood two full cycles of 8% drift ratio without any strength degradation. However, the longitudinal bars fractured during the following loading cycle of 10% drift. The CIP S1-Bond, and PDC columns withstood one full cycle of 10% drift followed by bar fracture at the second cycle of the 10% drift ratio. The drift capacities for the CIP, PNC, S1-Bond and PDC were 9.93%, 8.96%, 10.42% and 10.29%, respectively.

Table 4.1- Displacement Capacity for All Column Models.

Column model	First yield point			Effective yield point			Ultimate Point			Disp. Ductility capacity
	Disp., (in)	Drift, (%)	Force, (kips)	Disp., (in)	Drift, (%)	Force, (kips)	Disp., (in)	Drift, (%)	Force, (kips)	
CIP	0.86	0.79	38.8	1.46	1.35	66	10.7	9.93	68.5	7.36
PNC	0.96	0.89	40.3	1.54	1.42	63.7	9.67	8.96	56.24	6.3
S1-Bond	0.731	0.84	28.57	1.29	1.48	50.5	9.06	10.42	44.68	7.02
PDC	1.074	1.23	41.15	1.25	1.44	49.5	8.95	10.29	41.56	7.13

The normalized average push and pull force-drift envelopes for all the column models is shown in Figure 4.24. It is observed that all the columns incorporating the filled duct connections had reached their lateral load capacities without any strength degradation at 8% drift while the CIP column reached its load capacity at 10% drift. Overall, the PDC, PNC and CIP column models showed almost the same normalized average envelope, while the S1-Bond column model showed an overall softer behavior compared to the other three column models. This is attributed to the fact that the column-footing interface was not well prepared to ensure full contact between both members which affected the overall force-drift response by inducing higher end rotations at lower drift ratios resulting in lower lateral force readings. This specific observation is what support the recommendation previously mentioned in the construction discussion, i.e. Polymer concrete overflow or bedding layer is strongly recommended to be used for bedding when precast columns are installed into the footing.

Table 4.1 provides the displacement capacities for all the column models. The displacement ductility capacities for the CIP, PNC, S1-Bond and PDC were 7.36, 6.30, 7.02 and 7.13, respectively. The PDC, S1-Bond and the CIP column models showed a very close ductility capacities while the PNC column model had a lower ductility capacity than the CIP with 14% difference, respectively. The lower displacement ductility capacity of PNC could be attributed to

lower concrete compressive strength of the shell compared to the CIP column concrete, which slightly reduced the confinement effectiveness and resistance against bar buckling.

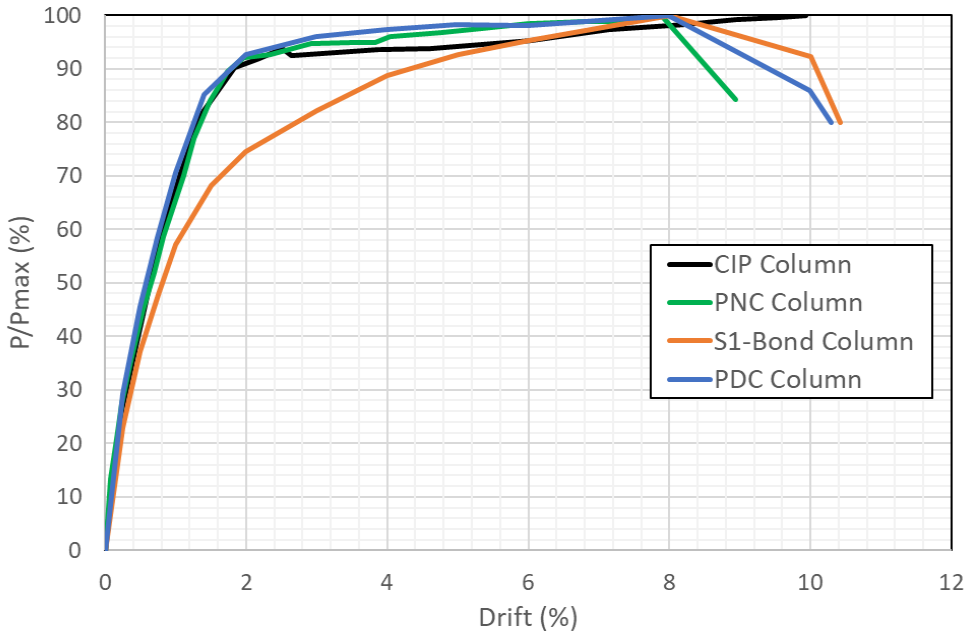

Figure 4.24 Normalized Average Push and Pull Force-drift Envelopes for all Column Models.

CHAPTER 5. SUMMARY AND CONCLUSIONS

5.1. Summary

Accelerated bridge construction (ABC) employs innovative detailing and planning as well as new construction techniques to accelerate construction. There are several advantages for implementing ABC in the building of new bridges or the rehabilitation and replacement of old deteriorated bridges, for instance: reducing onsite construction time which consequently reduce the traffic effects, and the improved quality of the prefabricated elements as they are typically constructed in prefabrication plants which usually impose high quality control measures. With the exponentially increasing numbers of bridges in the US, about 150,000 bridges in the US according to FHWA, which needs rehabilitation, repair, or total replacement, the ABC techniques has become a good and efficient alternative to the time-consuming cast-in-place (CIP) conventional construction. Implementing ABC techniques help decrease the economical, social, and construction costs or impact associated with long bridge construction duration.

Recently, The ABC applications has been widely implemented in low seismic regions of the country and mostly in the superstructure elements. However, it has not yet been extensively utilized in substructure elements such as column-base connections, especially in moderate and high seismic regions due to the uncertainty in the seismic performance of the substructure connections. A few ABC seismic connections were developed and have been examined for potential use in high seismic regions. Among these, grouted-ducts have been one of the most promising ABC connection types. However, past research utilized either proprietary and sole-sourced UHPC, or non-proprietary expensive and complexly mixed UHPC, which posed barriers toward wide-spread implementation grouted-ducts. To address this issue, the overall goal of this study was to implement the polymer concrete in grouted-duct ABC seismic connections of precast bridge columns that can emulate the seismic performance of conventional CIP columns.

This study revisited the previously developed UHPC-filled grouted-duct connection (Tazarv and Saiidi 2014, and Aboukifa et al. 2021) that has been used to connect precast columns to footings with the aim of utilizing a different grout. Reducing the mixing complexity, costs and accelerating the time consumed by the grouting material for the full-strength gain was the focus of this study to establish a less expensive, less restrictive, and more efficient alternative for UHPC-

filled grouted-duct connections. In this study, full comprehensive study of the main mechanical and structural properties of the polymer concrete was conducted. After observing satisfactory and promising performance of the polymer concrete (i.e., very easy mixing procedure, and full strength gain in less than 24-hours), it was used in grouted-duct connections in a large-scale (42%-scale) column model with a grouted duct precast column-to-footing connection. The column model was tested at UNR under combined axial and cyclic lateral loading to investigate its seismic performance and evaluate their ability to emulate the behavior of CIP column-footing connections.

5.2. Concluding Remarks

The findings from the mostly experimental study performed on the polymer concrete filled duct column-footing connection led to the following observations and concluding remarks:

1- The polymer concrete mix presented in this study is a less complex, low-cost, and efficient alternative to the normally used UHPC mixes to be used in the column-to-footing duct connections without increasing the required embedment length of the bars inside the ducts.

2- The polymer concrete filled duct connections presented in this study were emulative of conventional cast-in-place (CIP) column-to-footing connections as indicated by successfully developing the full columns ultimate strength capacities and achieving high drift capacities without connection damage. Accordingly, the precast columns incorporating the polymer concrete mix presented in this study can be designed in accordance to current bridge codes with no limitations.

3- The observed mode of failure for the PDC column model was confirmed to be full plastic hinge developed in the column outside the footing. The stages of the formed plastic hinge started with the column concrete cover spalling then followed by bars buckling and spirals rupture then finally longitudinal bars rupture. The duct connections exhibited no damage such as bar pullout, duct pullout, or conical failure of the footing, as per visual inspection and final status and view of the footing top surface, even at under 12% drift ratio.

4- The PDC column model was able to undergo large inelastic deformations with drift capacity of 10.3%, compared to 9.9%, 9% and 10.4% for the CIP (conventional column), PNC (column with proprietary UHPC filled ducts), and S1-Bond (column with nonproprietary UHPC filled ducts) column models, respectively. The measured displacement ductility capacity of PDC

column model was at least 7.1, which well exceeds the AASHTO requirements for ductility demand of 5.0 for single column bents.

5- Applying a leveling bedding layer at the interface between the column and the footing to ensure full contact between both members is found to be a successful technique in grouted-duct connections to maintain comparable initial stiffness and degradation behavior as CIP columns.

6- Overall, polymer concrete filled duct connections are recommended as suitable precast column-to-footing connections for moderate and high seismic regions because formation of full plastic moment in columns without any connection damage is assured.

REFERENCES

1. AASHTO. (2010). "AASHTO LRFD Bridge Design Specification," Washington, DC: American Association of State Highway and Transportation Officials.
2. Abokifa, M., Moustafa, M. A., & Itani, A. M. (2021). Comparative structural behavior of bridge deck panels with polymer concrete and UHPC transverse field joints. Engineering Structures, 247, 113195.
3. Abokifa, M., & Moustafa, M. A. (2021). Experimental behavior of poly methyl methacrylate polymer concrete for bridge deck bulb tee girders longitudinal field joints. Construction and Building Materials, 270, 121840.
4. Abokifa, M., & Moustafa, M. A. (2021). Mechanical characterization and material variability effects of emerging non-proprietary UHPC mixes for accelerated bridge construction field joints. Construction and Building Materials, 308, 125064.
5. Abokifa, M., & Moustafa, M. A. (2021). Experimental Behavior of Precast Bridge Deck Systems with Non-Proprietary UHPC Transverse Field Joints. Materials, 14(22), 6964.
6. Aboukifa, M., Moustafa, M. A., & Saiidi, M. S. (2021). Seismic response of precast bridge columns with composite non-proprietary UHPC filled ducts ABC connections. *Composite Structures*, *274*, 114376.
7. Aboukifa, M., Moustafa, M. A., & Saiidi, M. S. (2020). SEISMIC RESPONSE OF PRECAST COLUMNS WITH NON-PROPRIETARY UHPC-FILLED DUCTS ABC CONNECTIONS.
8. Aboukifa, M., Moustafa, M. A., Itani, A. M., & Naeimi, N. (2019). Durable UHPC Columns with High-Strength Steel (No. ABC-UTC-2013-C3-UNR02-Final). Accelerated Bridge Construction University Transportation Center (ABC-UTC).
9. Aboukifa, M., Moustafa, M., & Itani, A. (2019, June). Behavior of UHPC Column Subjected to Combined Axial and Lateral Loading. In International Interactive Symposium on Ultra-High Performance Concrete (Vol. 2, No. 1). Iowa State University Digital Press.
10. Aboukifa, M., Moustafa, M. A., & Itani, A. (2020). Comparative structural response of UHPC and normal strength concrete columns under combined axial and lateral cyclic loading. Special Publication, 341, 71-96.

11. Aboukifa, M., & Moustafa, M. A. (2021). Experimental seismic behavior of ultra-high performance concrete columns with high strength steel reinforcement. Engineering Structures, 232, 111885.

12. ACI Committee 239. (2012). "Ultra-High Performance Concrete," ACI Fall Convention, Toronto, Ontario, Canada.

13. ACI318. (2011). "Building Code Requirements for Reinforced Concrete," Detroit, Michigan: American Concrete Institute.

14. ACI408R-03. (2003). "Bond and Development of Straight Reinforcing Bars in Tension," ACI Committee 408, 49 pp.

15. Ameli, M.J., Parks, J.E., Brown, D.N., and Pantelides, C.P. (2014). "Grouted Splice Sleeve Connection Alternatives for Precast Reinforced Concrete Bridge Piers in Moderate-to-High Seismic Regions," *Proceeding of Tenth U.S. National Conference on Earthquake Engineering*, Anchorage, Alaska, 10 pp.

16. ASTM A615/A615M-09b. (2009). "Standard Specification for Deformed and Plain Carbon-Steel Bars for Concrete Reinforcement," West Conshohocken, PA, 6 pp.

17. ASTM A706/A706M-09b. (2009). "Standard Specification for Low-Alloy Steel Deformed and Plain Bars for Concrete Reinforcement," West Conshohocken, PA, 6 pp.

18. ASTM C109/C109M-11b. (2011). "Standard Test Method for Compressive Strength of Hydraulic Cement Mortars (Using 2-in. or [50-mm] Cube Specimens)," West Conshohocken, PA, 10 pp.

19. ASTM C39/C39M-12. (2012). "Standard Test Method for Compressive Strength of Cylindrical Concrete Specimens," West Conshohocken, PA, 7 pp.

20. Belleri, A., & Riva, P. (2012). Seismic performance and retrofit of precast concrete grouted sleeve connections.

21. Brenes, F.J., Wood, S.L. and Kreger, M.E. (2006). "Anchorage Requirements for Grouted Vertical-Duct Connectors in Precast Bent Cap Systems," *FHWA/TX-06/0-4176-1*, Center for Transportation Research, University of Texas at Austin.

22. Caltrans. (2006). “Seismic Design Criteria (SDC),” version 1.4. Sacramento, CA.: California Department of Transportation.

23. Caltrans. (2010). “Seismic Design Criteria (SDC),” version 1.6. Sacramento, CA.:California Department of Transportation,.

24. CEB-FIB. (1993). “CEB-FIB Model Code 1990: Design Code Committee EURO International Du Buton,” London, UK: Thomas Telford.

25. Cruz Noguez C.A. and Saiidi, M.S. (2012). “Shake Table Studies of a 4-Span Bridge Model with Advanced Materials,” *Journal of Structural Engineering, ASCE,* Vol. 138, No. 2, pp. 183-192.

26. Culmo, M. (2009). “Connection Details for Prefabricated Bridge Elements and Systems,” Federal Highway Administration *Report No. FHWA-IF-09-010*.

27. Culmo, M. P. (2011). “Accelerated Bridge Construction - Experience in Design, Fabrication and Erection of Prefabricated Bridge Elements and Systems,” Federal Highway Administration *Report No. FHWA-HIF-12-013*.

28. Eligehausen, R., Popov, E.P. and Bertero, V.V. (1982). “Local Bond Stress-Slip Relationships of Deformed Bars under Generalized Excitations,” *Proceedings of the 7th European Conference on Earthquake Engineering*. Vol. 4. Athens: Techn. Chamber of Greece. pp. 69-80.

29. Galvis, F., Correal, J.F., Betancour, N., and Yamin, L. (2015). "Characterization of the Seismic Behavior of a Column-Foundation Connection for Accelerated Bridge Construction," VII Congreso Nacional de Ingenieria Sismica, Bogota, Colombia, 10pp.

30. Graybeal, B. (2006). “Material Property Characterization of Ultra-High Performance Concrete,” McLean, VA: FHWA, U.S. Department of Transportation, *Report No. FHWA-HRT-06-103*.

31. Graybeal, B. (2010). “Behavior of Field-Cast Ultra-High Performance Concrete Bridge Deck Connections under Cyclic and Static Structural Loading,” Federal Highway Administration *Report No. FHWA-HRT-11-023*.

32. Graybeal, B. and Davis, M. (2008). “Cylinder or Cube: Strength Testing of 80 to 200 MPa (11.6 to 29 ksi) Ultra-High-Performance Fiber-Reinforced Concrete,” *ACI Materials Journal*, Vol. 105, No. 6, pp. 603-609.

33. Haber, Z. (2013). “Precast Column-Footing Connections for Accelerated Bridge Construction in Seismic Zones,” PhD Dissertation, University of Nevada Reno, 612 pp.

34. Haber, Z.B., Saiidi, M.S. and Sanders, D.H. (2013). “Precast Column-Footing Connections for Accelerated Bridge Construction in Seismic Zones,” Center for Civil Engineering Earthquake Research, Department of Civil and Environmental Engineering, University of Nevada, Reno, Nevada, *Report No. CCEER-13-08*, 502 pp.

35. Haber, Z.B., Saiidi, M.S. and Sanders, D.H. (2014). “Seismic performance of precast columns with mechanically spliced column-footing connections. ACI Struct J 2014;111(3):339–650.

36. Haraldsson, O.S., Janes, T.M., Eberhard, M.O. and and Stanton, J.F. (2012). “Seismic Resistance of Socket Connection between Footing and Precast Column,” *Journal of Bridge Engineering, ASCE*, Vol. 18, No. 9, pp. 910-919.

37. JSCE Concrete Library 127. (2008). “Recommendations for Design and Construction of High Performance Fiber Reinforced Cement Composites with Multiple Fine Cracks (HPFRCC),” Japan Society of Civil Engineers.

38. Khaleghi, B., Schultz, E., Seguirant, S., Marsh, L., Haraldsson, O., Eberhard, M. and Stanton, J. (2012). “Accelerated Bridge Construction in Washington State: From research to Practice,” *PCI Journal*, pp 34-49.

39. Mander, J.B., Priestley, M.J.N., Park, R. (1988). “Theoretical Stress-Strain Model for Confined Concrete,” *Journal of Structural Engineering, ASCE*, Vol. 114, No. 8, pp. 1804-1826.

40. Mantawy, I. M., Thonstad, T., Sanders, D. H., Stanton, J. F., & Eberhard, M. O. (2016). Seismic performance of precast, pretensioned, and cast-in-place bridges: Shake table test comparison. Journal of Bridge Engineering, 21(10), 04016071.

41. Marsh, M.L., Wernli, M., Garrett, B.E., Stanton, J.F., Eberhard, M.O. and Weinert, M.D. (2011). “Application of Accelerated Bridge Construction Connections in Moderate-to-High

Seismic Regions," Washington, D.C.: *National Cooperative Highway Research Program (NCHRP) Report No. 698*.

42. Matsumoto, E.E., Waggoner, M.C., Sumen, G. and Kreger, M.E. (2001). "Development of a Precast Bent Cap System," Center for Transportation Research, The University of Texas at Austin: *FHWA Report No. FHWA/TX-0-1748-2*.

43. Mehrsoroush, A. and Saiidi, M.S. (2014). "Seismic Performance of Two-Column Bridge Piers with Innovative Precast Members and Pipe Pin Connections," *Proceeding of 7th International Conference on Bridge Maintenance, Safety and Management (IABMAS)*, Shanghai, China.

44. Mo, Y.L., and Chan, J. (1996). "Bond and Slip of Plain Rebars in Concrete," *Journal of Materials in Civil Engineering, ASCE,* Vol. 8, No.4, pp. 208-211.

45. Monti, G., and Spacone, E. (2000). "Reinforced Concrete Fiber Beam Element with Bond-Slip," *Journal of Structural Engineering, ASCE,* Vol. 126, No. 6, pp. 654-661.

46. Motaref, S., Saiidi, M.S., and Sanders, D. (2011). "Seismic Response of Precast Bridge Columns with Energy Dissipating Joints," Center for Civil Engineering Earthquake Research, Department of Civil and Environmental Engineering, University of Nevada, Reno, *Report No. CCEER-11-01*.

47. OpenSees. (2013). "Open System for Earthquake Engineering Simulations," Version 2.4.1, Berkeley, CA, Available online: http://opensees.berkeley.edu.

48. Pang, J. B., Steuck, K. P., Cohagen, L., Eberhard, M. O., & Stanton, J. F. (2008). *Rapidly constructible large-bar precast bridge-bent connection* (No. WA-RD 684.2).

49. Popa, V., Papurcu, A., Cotofana, D., & Pascu, R. (2015). Experimental testing on emulative connections for precast columns using grouted corrugated steel sleeves. *Bulletin of Earthquake Engineering*, *13*(8), 2429-2447.

50. Raynor, D.J., Lehman, D.E. and Stanton, J.F. (2002). "Bond-Slip Response of Reinforcing Bars Grouted in Ducts," ACI Structural Journal, Vol. 99, No. 5, pp. 568-576.

51. Restrepo, J.I., Tobolski, M.J. and Matsumoto, E.E. (2011). "Development of a Precast Bent Cap System for Seismic Regions," *NCHRP Report 681*, Washington, D.C.

52. Russell, H.G. and Graybeal B.A. (2013). “Ultra-High Performance Concrete: A State-of-the-Art Report for the Bridge Community,” Federal Highway Administration, *Report No. FHWA-HRT-13-060*, 171 pp.

53. SETRA-AFGC. (2002). “Ultra High Performance Fibre-Reinforced Concretes,” Interim Recommendations, SETRA-AFGC, Groupe de travail BFUP, Paris, France, 98 pp.

54. Shrestha, G., Saiidi, M.S., Itani, A.M., and Sanders, D.H. (2018). “Seismic Studies of Superstructure and Substructure Connections for Accelerated Bridge Construction, Dissertation, University of Nevada, Reno

55. Soroushian, P. and Choi, K.B. (1989). “Local Bond of Deformed Bars with Different Diameters in Confined Concrete,” *ACI Structural Journal*, Vol. 86, No.2, pp. 217-222.

56. Steuck, K.P., Eberhard, M.O. and Stanton, J.F. (2009). “Anchorage of Large- Diameter Reinforcing Bars in Ducts,” *ACI Structural Journal*, Vol. 106, No. 4, pp. 506-513.

57. Steuck, K.P., Pang, J.B.K., Eberhard, M.O. and Stanton, J.F. (2008). “Anchorage of Large-diameter Reinforcing Bars Grouted into Ducts,” *WA-RD 684.1*, University of Washington, Seattle, Washington.

58. Subedi, D., Moustafa, M.A., and Saiidi, M.S. (2019). “Non-Proprietary UHPC for Anchorage of Large Diameter Column Bars in Grouted Ducts”. Center for Civil Engineering Earthquake Research, Department of Civil and Environmental Engineering, University of Nevada, Reno, Nevada, Report No. CCEER-19-06; 2019.

59. Thonstad, T., Mantawy, I. M., Stanton, J. F., Eberhard, M. O., & Sanders, D. H. (2016). Shaking table performance of a new bridge system with pretensioned rocking columns. Journal of Bridge Engineering, 21(4), 04015079.

60. Tazarv, M., and Saiidi M.S. (2014). “Next generation of bridge columns for accelerated bridge construction in high seismic zones”. Center for Civil Engineering Earthquake Research, Department of Civil and Environmental Engineering, University of Nevada, Reno, Nevada, Report No. CCEER-14-06; 2014. 400pp.

61. Tazarv, M., and Saiidi, M. S. (2015). “UHPC-filled duct connections for accelerated bridge construction of RC columns in high seismic zones.” Eng. Struct., 99(3), 413–422.

62. Utah Department of Transportation. (2010). “Precast Substructure Elements,” http://dot.utah.gov, 24 pp.

63. Wang, J.C., Ou, Y.C., Chang, K.C., and Lee, G.C. (2008). “Large-Scale Seismic Tests of Tall Concrete Bridge Columns with Precast Segmental Construction,” *Earthquake Engineering and Structural Dynamics*, Vol. 37, pp. 1449-1465.